

# Lipid composition greatly affects the *in vitro* surface activity of lung surfactant protein mimics

Shannon L. Seuryneck-Servoss<sup>a</sup>, Nathan J. Brown<sup>a</sup>, Michelle T. Dohm<sup>b</sup>,  
Cindy W. Wu<sup>a</sup>, Annelise E. Barron<sup>a,\*</sup>

<sup>a</sup> Department of Chemical and Biological Engineering, Northwestern University, 2145 Sheridan Road, Evanston, IL 60208, United States

<sup>b</sup> Department of Chemistry, Northwestern University, 2145 Sheridan Road, Evanston, IL 60208, United States

Received 8 October 2006; received in revised form 2 January 2007; accepted 3 January 2007

Available online 12 January 2007

## Abstract

A crucial aspect of developing a functional, biomimetic lung surfactant (LS) replacement is the selection of the synthetic lipid mixture and surfactant proteins (SPs) or suitable mimics thereof. Studies elucidating the roles of different lipids and surfactant proteins in natural LS have provided critical information necessary for the development of synthetic LS replacements that offer performance comparable to the natural material. In this study, the *in vitro* surface-active behaviors of peptide- and peptoid-based mimics of the lung surfactant proteins, SP-B and SP-C, were investigated using three different lipid formulations. The lipid mixtures were chosen from among those commonly used for the testing and characterization of SP mimics—(1) dipalmitoyl phosphatidylcholine:palmitoyloleoyl phosphatidylglycerol 7:3 (w/w) (PCPG), (2) dipalmitoyl phosphatidylcholine:palmitoyloleoyl phosphatidylglycerol:palmitic acid 68:22:9 (w/w) (TL), and (3) dipalmitoyl phosphatidylcholine:palmitoyloleoyl phosphatidylcholine:palmitoyloleoyl phosphatidylglycerol:palmitoyloleoyl phosphatidylethanolamine:palmitoyloleoyl phosphatidylserine:cholesterol 16:10:3:1:3:2 (w/w) (IL). The lipid mixtures and lipid/peptide or lipid/peptoid formulations were characterized *in vitro* using a Langmuir–Wilhelmy surface balance, fluorescent microscopic imaging of surface film morphology, and a pulsating bubble surfactometer. Results show that the three lipid formulations exhibit significantly different surface-active behaviors, both in the presence and absence of SP mimics, with desirable *in vitro* biomimetic behaviors being greatest for the TL formulation. Specifically, the TL formulation is able to reach low-surface tensions at physiological temperature as determined by dynamic PBS and LWSB studies, and dynamic PBS studies show this to occur with a minimal amount of compression, similar to natural LS.

© 2007 Elsevier B.V. All rights reserved.

**Keywords:** SP-B; SP-C; Pulsating bubble surfactometer; Langmuir–Wilhelmy surface balance

## 1. Introduction

Lung surfactant (LS), a complex biomaterial that coats internal pulmonary surfaces, is essential for normal breathing [1]. This surface-active material functions to reduce and regulate surface tension within the alveoli during respiration [1]. The most important attributes of LS are its ability to (i) adsorb rapidly to the air–water interface, (ii) reach near-zero surface tension upon film compression, preventing alveolar collapse, and (iii) respread at the air–water interface through multiple expansions and contractions of film surface area. The absence

or dysfunction of LS results in neonatal respiratory distress syndrome (nRDS), a leading cause of infant mortality in the United States [2]. Currently, premature infants suffering from nRDS are treated by intratracheal instillation of an exogenous LS replacement, typically animal-derived, into the lungs [3]. However, there are significant concerns associated with the use of animal-derived LS replacements, including high production and purification costs, batch-to-batch variability, and the potential for pathogen transmission [3]. Less expensive, synthetic LS replacements have been developed, but are not commonly used due to their generally inferior efficacy in the treatment of nRDS [3]. This poor performance is attributed to the lack of the hydrophobic surfactant proteins (SPs) present in animal-derived surfactant that are necessary for the proper biophysical functioning of LS [3]. Hence, there is a need for a safe, cost-effective,

\* Corresponding author. Tel.: +1 847 491 2778; fax: +1 847 491 3728.  
E-mail address: [a-barron@northwestern.edu](mailto:a-barron@northwestern.edu) (A.E. Barron).

entirely synthetic LS replacement that contains good functional mimics of both the hydrophobic SPs and the lipid portion of LS.

In order to create a useful synthetic LS replacement, the role of each LS component must be considered carefully. Lipids comprise approximately 90% of LS by weight, and SPs approximately 10% [1]. The hydrophobic SPs, SP-B and SP-C, are thought to be critical for facilitating the proper interfacial lipid dynamics and maintaining respreadability of the lipid film [3]. The addition of SP-B and/or SP-C to natural or synthetic lipid mixtures results in a faster rate of adsorption, lower minimum surface tensions, and better respreadability of the film compared to the film without added SP [4].

The major lipid class in LS is phosphatidylcholine (PC), which comprises approximately 65–75% of LS lipids; dipalmitoyl phosphatidylcholine (DPPC) is the most prevalent single component of LS, comprising 40–60% of the PC species. Monolayers of DPPC are able to maintain near-zero surface tensions upon compression due to the tight packing ability of saturated phospholipids [4]. However, this stiff and rigid monolayer adsorbs slowly to the air–aqueous interface and respreads poorly upon successive compressions and expansions of film area [4]. The addition of unsaturated phospholipids such as palmitoyloleoyl phosphatidylcholine (POPC) and palmitoyloleoyl phosphatidylglycerol (POPG) or other lipids and hydrophobic molecules such as palmitic acid (PA) and cholesterol has been shown to enhance the adsorption rate of the lipid film as well as improve its respreadability; however, the minimum surface tension upon compression is thus increased relative to DPPC films [5].

There is growing evidence that a functional replacement for natural LS must either contain SP-B and/or SP-C or comprise good functional mimics of these small, amphipathic proteins. Both have unique structural attributes that are not trivial to mimic with synthetic peptides or peptidomimetics. SP-B is an amphipathic, predominantly helical protein that is 79 amino acids long [4], with three intramolecular disulfide bridges [6] and one intermolecular disulfide bond, forming a homodimer [4]. SP-B knockout mice die at birth [7]; however, since SP-B is necessary for the processing of SP-C proprotein, these mice also lack functional SP-C [8]. SP-B directs LS surface activity through the control of lipid film organization [4] and enhances monolayer adsorption and resreading [4]. While the chemical synthesis of an exact mimic of this 79mer protein is too difficult to be practical, there is evidence, based on Langmuir trough studies, that the cationic, helical amino-terminal region, SP-B<sub>1–25</sub>, retains much of the physiological function of synthetic SP-B<sub>1–78</sub> (direct comparisons to the natural protein have not been published) [9,10].

SP-C is an exceedingly hydrophobic, amphipathic, helical protein, comprised of 35 amino acids [4]. SP-C contains two cationic residues at positions 11 and 12 that interact with anionic phospholipid head groups of a lipid film [11] and post-translationally palmitoylated cysteines at positions 5 and 6 that are believed to be important for proper function; however, their exact role and the extent of their importance are a matter of debate [12–16]. SP-C's structure is dominated by an  $\alpha$ -helix that is approximately 37 Å long, and within this helical region is

a 23 Å-long, valyl-rich stretch of hydrophobic amino acids. The lengths of the helix and valyl-rich region closely match the thickness of a DPPC bilayer and its acyl chain portion, respectively, suggesting that SP-C can traverse a phospholipid bilayer [17], or form a transbilayer orientation, interacting with the hydrophobic lipid acyl chains [18]. Due to extreme hydrophobicity and a strong tendency to aggregate and misfold in the absence of lipids, several simplified peptide mimics of SP-C have been created and studied [19–23]. Takei et al. synthesized various non-palmitoylated, full-length and truncated forms of SP-C, and found that a core sequence (residues 5–31 or 6–32) is required for biophysical activity comparable to the full-length protein [22]. Nilsson et al. created an SP-C analog by replacing valines with leucines and cysteines with serines, which showed surface activity comparable to native SP-C, but with a much-reduced tendency for hydrophobic aggregation and misfolding [24,25].

In previous studies, we have investigated the surface-active behaviors of peptoid-based mimics of both SP-B and SP-C in lipid films, and compared the activity of the peptoids to the respective peptide mimics [26,27]. Peptoids represent an alternate derivative of a polypeptide backbone, with the side chains attached to the amide nitrogens rather than to the  $\alpha$ -carbons [28,29]. The *N*-substituted backbone of this class of molecules resists proteolysis, resulting in enhanced bioavailability and the potential for reduced specific recognition by the immune system [30,31]. Such properties are of course extremely sequence- and size-dependent, and the biocompatibility of longer peptoid oligomers has not yet been assessed. Although peptoids are not able to form backbone–backbone hydrogen bonds like peptides to stabilize secondary structure [32], structural studies have shown that peptoid sequences with homochiral side chains form stable helical structures with a chiral sense, similar to polyproline helices in peptides [33]. Peptoid helices have a helical pitch of approximately 6 Å and a periodicity of three residues per turn, and are stabilized primarily by steric and electronic repulsions [32].

Both peptoid-based SP mimics we previously reported were designed to capture the essential structural features of the cognate peptide: SP-B mimics were helical and facially amphipathic [26], while SP-C mimics were helical and longitudinally amphipathic [27]. The surface-active behaviors of the peptoid mimics as well as of comparator peptides were characterized in biomimetic lipid films using a Langmuir–Wilhelmy surface balance (LWSB) and a pulsating bubble surfactometer, while film phase morphologies were observed using fluorescence microscopy in conjunction with an LWSB. The peptoid mimics were found to exhibit surface-active behaviors and film phase morphologies that were in many ways similar to, though not identical to the model peptide mimics [26,27].

It has been shown that lipid composition can play an important role in the surface activity and structure of SP mimics in a lipid film [34]. In this study, we examine the *in vitro* function of two peptide- and two peptoid-based SP mimics in three different lipid formulations to further investigate SP mimic/lipid interactions. The lipid mixtures were chosen from among those commonly used for the testing and characterization of SP mimics—(1) dipalmitoyl phosphatidyl-

choline:palmitoyloleoyl phosphatidylglycerol 7:3 (w/w) (PCPG), (2) dipalmitoyl phosphatidylcholine:palmitoyloleoyl phosphatidylglycerol:palmitic acid 68:22:9 (w/w) (TL), and (3) dipalmitoyl phosphatidylcholine:palmitoyloleoyl phosphatidylcholine:palmitoyloleoyl phosphatidylglycerol:palmitoyloleoyl phosphatidylethanolamine:palmitoyloleoyl phosphatidylserine:cholesterol 16:10:3:1:3:2 (w/w) (IL). To our knowledge, this is the first time a comparative study such as this has been completed for peptidomimetic molecules and the respective peptides that they mimic. Our results show that these three lipid formulations exhibit significantly different surface-active behaviors as determined by LWSB, FM, and PBS studies, both in the presence and absence of SP mimics. Additionally, we find that lipid composition has dramatic effects on the surface-active behaviors of both peptoid- and peptide-based SP mimics, which has important implications for their use in biomimetic LS replacement formulations.

## 2. Materials and methods

### 2.1. Materials and reagents

Peptide and peptoid synthesis reagents were purchased from Applied Biosystems (Foster City, CA) and Aldrich (Milwaukee, WI). Resins and Fmoc-protected amino acids were purchased from NovaBiochem (San Diego, CA), while 2,2,5,7,8-pentamethylchroman-6-sulfonyl chloride (PMC) was purchased from Omega Chemical (Quebec, CA), and primary amines and di-*tert*-butyl dicarbonate (Boc) were purchased from Aldrich. Acetonitrile, isopropanol, and trifluoroacetic acid (TFA) were purchased from Fisher Scientific (Pittsburgh, PA). DPPC, POPG, POPC, POPE, POPS, and cholesterol were purchased

from Avanti Polar Lipids (Alabaster, AL), PA was purchased from Aldrich, and Texas Red<sup>®</sup> 1,2-dihexadecanoyl-*sn*-glycero-3-phosphoethanolamine, triethylammonium salt (TR-DHPE) was purchased from Molecular Probes (Eugene, OR). All chemicals were purchased in high purity form and were used without further purification.

### 2.2. Peptide and peptoid synthesis, purification, and characterization

Cysteine-to-alanine substitutions were made at positions 8 and 11 in the peptide SP-B<sub>1–25</sub> to prevent unwanted disulfide bond formation (Table 1). We synthesized a non-palmitoylated SP-C-mimetic peptide with a sequence modified to prevent aggregation and preserve the hydrophobicity of the *N*-terminal region, SP-C<sub>FF</sub>, which included valine-to-leucine and cysteine-to-phenylalanine substitutions (sequence shown in Table 1) [25,35]. Both peptides were synthesized by standard Fmoc chemistry on solid support (pre-loaded Wang resin) using an ABI 433A automated peptide synthesizer (Applied Biosystems).

A peptoid-based mimic of SP-B, Peptoid B, was designed to mimic the helicity, cationic charge, facial amphipathicity, and hydrophobicity of SP-B<sub>1–25</sub>, as previously described (structure shown in Table 1) [26]. A peptoid mimic of SP-C, Peptoid C, mimics residues 5–32 from human SP-C, with close sequence mimicry at the *N*-terminus and maintenance of the C-terminal hydrophobic helix (structure shown in Table 1) [27]. Both peptoids were synthesized using an ABI 433A on Rink amide resin by the sub-monomer protocol as previously described [29]. All molecules were cleaved from the resin with TFA, along with the appropriate scavenging reagents, for 10 min or 1 h depending on the sequence (the longer time is necessary to remove the PMC

Table 1  
Peptide and peptoid sequences and molecular weights

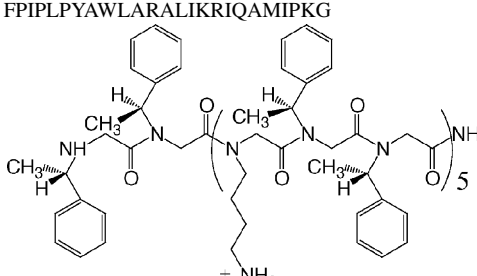
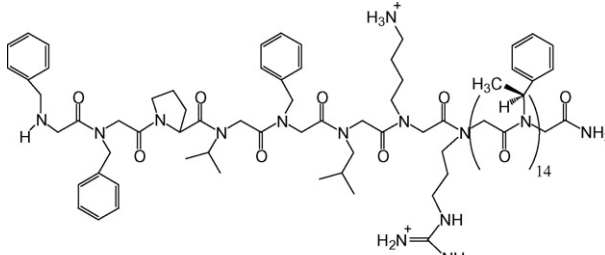
Molecule	Sequence/structure	Molecular weight (Da)
SP-B <sub>1–25</sub>	FPIPLPYAWLARALIKRIQAMIPKG	2866
Peptoid B		2592
SP-C <sub>FF</sub>	FGIPFFPVHLKRLILLLLLLLLLLLLLLILGALLMGL	3924
Peptoid C		3309

Table 2  
Molar percentages of added peptide or peptoid in each lipid formulation

	PCPG (mol%)	TL (mol%)	IL (mol%)
SP-B <sub>1-25</sub> /Peptoid B	2.5	2.2	2.4
SP-C <sub>FF</sub> /Peptoid C	1.9	1.6	1.8

protecting group from guanidine side chains in the acid-stable SP-B<sub>1-25</sub> and SP-C<sub>FF</sub>, peptides). SP-B mimics were purified by reversed-phase high performance liquid chromatography (RP-HPLC) using a linear gradient of 20–95% solvent B in solvent A over 50 min (solvent A is 0.1% TFA in water (v/v) and solvent B is 0.1% TFA in acetonitrile (v/v)). SP-C mimics were purified by RP-HPLC using a linear gradient of 30–80% solvent B in solvent A over 50 min (solvent A is 0.1% TFA in water (v/v) and solvent B is 0.1% TFA in acetonitrile–isopropanol 1:1 (v/v) for Peptoid C and 0.1% TFA in isopropanol (v/v) for SP-C<sub>FF</sub>). The final purities of the molecules were confirmed to be >97% by analytical RP-HPLC, and molecular weights were confirmed by electrospray ionization mass spectrometry (Table 1). The extent of helicity of the peptides and peptoids was confirmed by circular dichroism spectroscopy [26,27].

### 2.3. Methods and apparatus

#### 2.3.1. Sample preparation

Each lipid was individually dissolved in chloroform/methanol (3/1 (v/v)) to a precisely known concentration (~4 mg/mL). The lipids were then combined to make three different formulations, which we named: “PCPG lipids” (DPPC:POPG, PCPG, 7:3 (w/w)), “Tanaka lipids” (TL, DPPC:POPG:PA, 68:22:9 (w/w)), and “synthetic Infasurf lipids” (IL, DPPC:POPG:POPE:POPS:cholesterol, 16:10:3:1:3:2 (w/w)) with total lipid concentrations of ~2 mg/mL.

Peptide and peptoid mimics were dissolved in methanol to a known concentration (~2 mg/mL). The modified peptides, SP-B<sub>1-25</sub> and SP-C<sub>FF</sub>, were added to the lipid mixtures at 10 wt.%, which is similar to the total protein content in LS. The peptoid mimics were added to the lipids at equivalent mole percentages (see Table 2) comparable to those used in other studies [36].

#### 2.3.2. Langmuir–Wilhelmy surface balance studies

Surface pressure–molecular area isotherms were obtained using a home-built Langmuir–Wilhelmy surface balance, as previously described [26]. The trough was filled with 300 mL of aqueous buffer (150 mM NaCl, 5 mM CaCl<sub>2</sub>, 10 mM HEPES, pH 6.9) and heated to either 25 or 37 °C. The surfactant formulation was spread at the air–water interface from a chloroform/methanol solution using a glass syringe and allowed to equilibrate for 5 min. The barriers were then compressed and expanded at a rate of 30 mm/min. Surface pressure was measured using a Wilhelmy plate (Riegler and Kirsten GMBH, Berlin). The average surface area per molecule was calculated including both the lipids and the protein mimics. Experiments were repeated a total of six times per temperature for each surfactant formulation and gave reproducible results. Error bars fall within the thickness of the lines.

#### 2.3.3. Fluorescence microscopic imaging

In order to obtain fluorescence microscopic images of the lipid films on the Langmuir trough, a Nikon MM40 compact microscope stand with a 100 W mercury lamp (Tokyo, Japan) was used in conjunction with an LWSB. Fluorescence was detected by a Dage-MTI three-chip color camera (Dage-MTI, Michigan City, IN) in conjunction with a generation II intensifier (Fryer, Huntley, IL). Samples were spiked with 0.5 mol% of a fluorescently labeled lipid, TR-DHPE, for detection. Previous studies have shown that inclusion of the labeled lipid at this concentration does not alter surfactant film morphology [37]. Experiments were performed on an aqueous buffered subphase at 25 and 37 °C with a barrier speed of 5 mm/min, and were repeated a total of three times per temperature for each surfactant formulation; results were reproducible.

#### 2.3.4. Pulsating bubble surfactometry

A modified pulsating bubble surfactometer (General Transco, Largo, FL), which has been previously described [38], was used to obtain both static-bubble and dynamic-bubble adsorption data. An image acquisition system has been added to a commercial PBS in order to track bubble shape and size in real time. Images and pressure data from the instrument are sent to a LabVIEW program that is used to fit the bubble to an ellipse and calculate both the surface tension and the surface area of the bubble, resulting in more accurate determination of bubble surface tension based on bubble size [38]. Some of the major differences observed with the image analysis system, relative to the simpler commercial system, are higher maximum surface tensions, reduced hysteresis in the data loop, and a reduced slope upon expansion of the bubble. These differences have been shown to reflect a more accurate measurement and representation of the surface-active behaviors of biomimetic LS formulations [38]. In addition, we are able to visually detect any movement (leakage) of surfactant up the capillary or formation of particulates in the sample. Runs that showed either of these phenomena were removed from further analysis.

Surfactant formulations were dried from the chloroform/methanol solution using a DNA 120 Speedvac (Thermo Electron, Holbrook, NY), forming a pellet. The pellet was suspended in an aqueous buffer (150 mM NaCl, 5 mM CaCl<sub>2</sub>, 10 mM HEPES, pH 6.9) to 1.0 mg lipid/mL, with a final volume of 70–80 μL. The surfactant formulations were mixed with a micropipette, sonicated briefly with a Fisher Model 60 probe sonicator, and then mixed with a micropipette again to form a uniform suspension. Samples were loaded into a plastic PBS sample chamber (General Transco) with putty placed on the capillary end of the sample chamber to prevent sample leakage; the putty was removed before experiments were performed [39].

All experiments were performed at physiological temperature, 37 °C. Static adsorption surface tension data were collected for 20 min or until equilibrium surface tension was reached, starting with a bubble radius of 0.4 mm and allowing the bubble size to drift (grow) throughout the adsorption period. Following static adsorption, dynamic adsorption data were obtained at a frequency of 20 cycles/min until the shape of the hysteresis loop remained unchanged for at least 2 min, again starting with a

minimum bubble radius of 0.4 mm and allowing the bubble size to drift (grow) throughout the experiment. PBS experiments were repeated a total of six times for each surfactant formulation, and gave reproducible results. The trends reported for both static and dynamic adsorption experiments were consistent with all repeated experiments for each surfactant formulation.

### 3. Results and discussion

#### 3.1. Comparison of the surface-active behavior of three synthetic lipid formulations commonly used as mimics of the non-protein portion of lung surfactant

##### 3.1.1. Composition and efficacy of each lipid formulation

The surface-active behavior of SP mimics can vary greatly with lipid composition, and therefore SP mimics have been characterized in a multitude of different lipid formulations, including pure monolayers of DPPC [12,40], dipalmitoyl phosphatidylglycerol (DPPG) [9,12], and PA [41]. Since both SP-B and SP-C are cationic and are thought to interact with anionic PG head groups [6,42–46] and since DPPC is necessary for reaching low-surface tensions, formulations composed of both DPPC and POPG have also often been used for the surfactometry characterization of SPs and their mimics in lipid films [47–52].

Tanaka et al. investigated 25 different surfactant formulations containing varying combinations of phospholipids (DPPC, PG, phosphatidylserine (PS), phosphatidylinositol (PI), phosphatidylethanolamine (PE), and sphingomyelin), fatty acids (PA, palmitoleic acid, stearic acid, or oleic acid), acylglycerols, and a lipid-bound protein isolated from LS [53]. Of these 25 formulations, they found three surfactant mixtures with good, apparently biomimetic, *in vitro* surface activities, all containing 68.6% DPPC, 22.2% PG or PS, 9.1% fatty acid (palmitic acid or stearic acid), and 0.9% protein (w/w). Based on these results, a similar lipid formulation containing DPPC, POPG, and PA (68:22:9 (w/w)), the so-called “Tanaka lipids” (TL) has since been used widely to investigate the surface activity of SP mimics both *in vitro* and in animal models of RDS [26,27,37,54–61].

While the Tanaka lipids have been shown to facilitate the biomimetic functioning of surfactant protein replacements both *in vivo* and *in vitro*, this simple formulation has a composition that differs greatly from that of natural lung surfactant lipids. Most notably, the DPPC content of the Tanaka lipids (69%) is significantly higher than that of natural LS and also of successful, commercially available LS replacements such as Infasurf<sup>TM</sup> (55%) [34]. In addition, the inclusion of PA in Tanaka lipids is highly debated; while PA does not comprise a significant portion of natural LS lipids and increases the viscosity of the lipid film, it has been successfully included in effective clinical preparations and widely used for both *in vitro* and *in vivo* testing. Natural LS also contains other anionic phospholipids that are likely to interact with the cationic amino acid side chains of SP-B and SP-C, such as PI, PE, and PS, as well as cholesterol, which is believed to contribute to fluidization of the lipid film [62–70]. Walther et al. recently investigated the surface activity of three lipid formulations, including (1) lipids isolated from lung lavage, (2) a more complex formulation designed to be the synthetic

equivalent of the natural LS lipids, and (3) the Tanaka lipids, in combination with dimeric SP-B<sub>1–25</sub> peptide both *in vitro* (captive bubble surfactometer) and *in vivo* (a rat washout model of RDS) [34]. Studies performed on the captive bubble surfactometer indicate that formulation (2), the synthetic lung lavage lipid formulation that more closely mimics the composition of natural lung lavage lipids, containing DPPC, DOPC, POPG, POPE, POPS, and cholesterol (16:10:3:1:3:2 (w/w)), reached a minimum surface tension similar to that of both natural lipids and the Tanaka lipids. In addition, studies in a rat model of RDS revealed higher oxygenation levels with the natural lipids or the synthetic lung lavage lipids than with the Tanaka lipids. Therefore, this synthetic lipid formulation that more closely mimics the composition of natural LS seems to show greater promise for *in vivo* use as part of a biomimetic LS replacement.

Here we have investigated the surface activities of four SP mimics, including both peptides and peptoids, in three different lipid formulations: “PCPG”, composed of DPPC and POPG (7:3 (w/w)); “Tanaka lipids (TL)”, composed of DPPC, POPG, and PA (68:22:9 (w/w)); and “synthetic Infasurf lipids (IL)”, based on the composition of the lipid portion of natural LS [34] and composed of DPPC, POPC, POPG, POPE, POPS, and cholesterol (16:10:3:1:3:2 (w/w)). The *in vitro* surface activities of the three lipid formulations, with and without added SP mimics, were investigated using a Langmuir–Wilhelmy surface balance (LWSB), fluorescence microscopic (FM) imaging, and a pulsating bubble surfactometer (PBS).

##### 3.1.2. Langmuir–Wilhelmy surface balance results

An LWSB is typically used to record surface pressure ( $\Pi$ )–molecular area ( $A$ ) isotherms. Lipids are spread at the air–aqueous interface in the 2D gas–liquid coexistence region, at a high enough molecular area so that the lipid tails do not interact with one another and the surface pressure is essentially independent of molecular area. As the barriers are compressed, lipid tails begin to interact, entering the liquid expanded (LE) phase, and an increase in surface pressure is observed (referred to as lift-off). For natural LS, lift-off is expected to occur at a high molecular surface area ( $>100 \text{ \AA}^2/\text{molecule}$ ) [71]. As the barriers are further compressed, a coexistence of LE and liquid condensed (LC) phases is observed. A biomimetic plateau in the isotherm between 40 and 50 mN/m, which is thought to correspond to a 2D phase transition and/or the structured removal of material from the monolayer [71], is typically observed for effective LS formulations. Finally, at high surface pressures the solid phase is observed, and for biomimetic LS formulations, we expect to see a collapse pressure near 70 mN/m corresponding to a surface tension near 0 mN/m [71].

$\Pi$ – $A$  isotherms taken at 25 °C for the three lipid formulations with no SP mimic added (Fig. 1A) reveal that TL exhibit a much later lift-off ( $\sim 95 \text{ \AA}^2/\text{molecule}$ ) than either PCPG or IL ( $\sim 110 \text{ \AA}^2/\text{molecule}$ ). This trend is also observed, though much less dramatically, at 37 °C (Fig. 1B), with a lift-off area of  $\sim 100 \text{ \AA}^2/\text{molecule}$  for TL,  $\sim 110 \text{ \AA}^2/\text{molecule}$  for PCPG, and  $\sim 120$  for IL. All  $\Pi$ – $A$  isotherms exhibit at least a small kink at  $\sim 55 \text{ mN/m}$  at 25 °C, with more pronounced plateaus for TL and IL; at 37 °C, all lipid formulations exhibit plateaus at  $\sim 50 \text{ mN/m}$ .

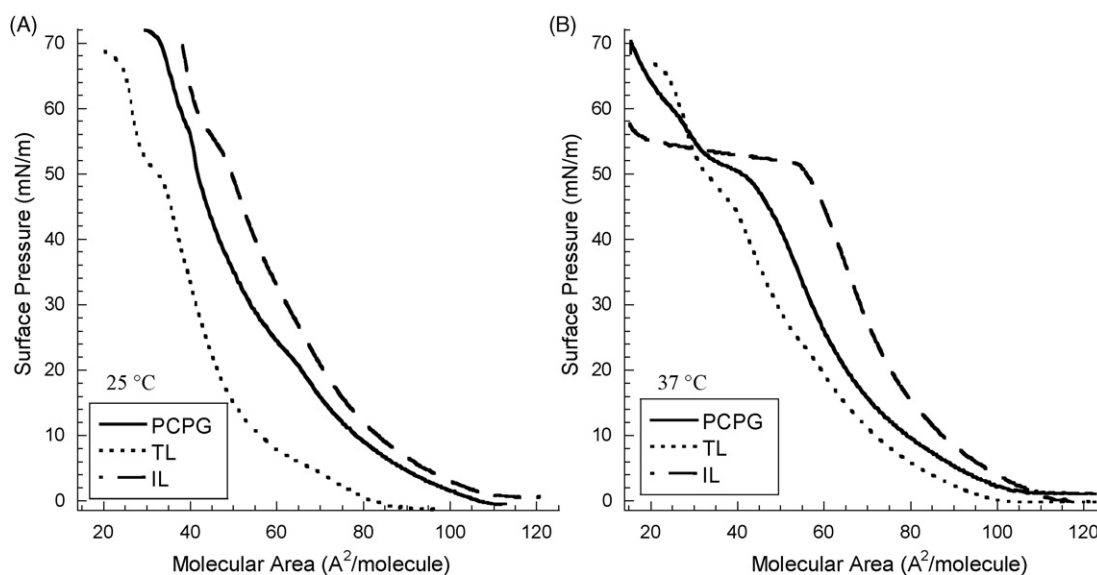


Fig. 1. Surface pressure–surface area isotherms obtained using the Langmuir–Wilhelmy surface balance at 25 °C (A) and 37 °C (B) for PCPG lipids, Tanaka lipids, and synthetic Infasurf lipids.

Finally, with the exception of IL at 37 °C, collapse pressures are near 70 mN/m. Interestingly, at 37 °C, the IL film exhibits a low collapse pressure, of approximately 55 mN/m. To our knowledge, this phenomenon has not previously been reported. While IL films have been previously studied, LWSB results were not reported by Walther et al. [34].

The later lift-off area observed with the TL film in comparison to those of PCPG and IL is likely due to the inclusion of PA in only the TL formulation. Because PA is a single-chain lipid with a small head group relative to DPPC or unsaturated phospholipids, it occupies less space in the monolayer and therefore it takes a greater degree of film compression for the lipid tails in the IL formulation to begin interacting with one another. Furthermore, IL contains more unsaturated lipids, which have kinked tails and take up more space in the monolayer, than either PCPG or TL (~49% for IL versus ~30% for PCPG and ~22% for TL), leading to lift-off at a higher molecular area for IL films. The inclusion of cholesterol and the increased percentage of unsaturated phospholipids in the IL formulation is known to fluidize lipid monolayers at higher surface pressures and temperatures [72]. This provides an explanation for why the IL lipid film is not able to reach high surface pressures, nor to make the transition from the LE/LC phase to a solid phase without film collapse, once the temperature is elevated to 37 °C.

### 3.1.3. Fluorescence microscopic imaging

The surface phase morphologies of the lipid films were observed using FM imaging in conjunction with the LWSB. FM images were obtained by spiking the samples prepared for LWSB studies with 0.5 mol% TR-DHPE. The bulky fluorescent tag is attached to the DHPE lipid head group, and resides predominantly in the LE phase, which appears as the bright regions in the images, while the probe excluded LC phase appears relatively dark. In all of the presented FM figures, the panels on the left (at lower surface pressure) depict films in that are either

entirely (PCPG and IL) or predominantly (TL) in the LE phase, and which therefore are quite bright in intensity. As surface pressure increases, the intensity of the fluorescent lipid in the LE phase typically decreases, and in the case of LC phases, the fluorescently labeled lipid is completely excluded from certain regions. As a result, the FM images on the right (at higher surface pressure) appear significantly darker overall, and when bright spots (termed ‘vesicles’ here) are present, the surrounding phases appear almost completely dark. In Fig. 2, FM images are shown for PCPG (A and B), TL (C and D), and IL (E and F) films at 37 °C, from a point on the isotherm just before the plateau, ~35 mN/m (left panels: A, C and E), and within the plateau, ~50 mN/m (right panels: B, D and F). At ~35 mN/m, no distinct LC domains are observed for either PCPG or IL, indicating that a fluid disordered LE phase is present, while dark LC domains are seen in the TL film. These domains in the TL film are consistent with the known DPPC:PA close packing that occurs in DPPC:PA and DPPC:POPG:PA films [37,73]. The lipid-fatty acid interactions promote mixed crystalline condensed solid phases that form in the non-condensable fluid phase, which contains POPG. Thus, LC domains are observed in TL, but not PCPG, films [37,73]. The IL film displays what appears to be a homogeneous fluid phase, though cholesterol is known to induce lipid-cholesterol short-range order almost independent of surface pressure over only a few molecules at a time [74]. At ~50 mN/m, some vesicle formation is observed for all of the lipid formulations (as evidenced by the appearance of small bright domains), and in the TL film, bright vesicle formations coexist with the dark LC domains. Interestingly, the fundamental phase morphologies at ~50 mN/m are very different for the three formulations. In the cases of both the PCPG and IL films, the vesicles are large and are likely forming below the monolayer [75], confirming that material is removed from the monolayer in the plateau region [76–78]. The TL film exhibits LC domains of about the same size as those observed at ~35 mN/m, but

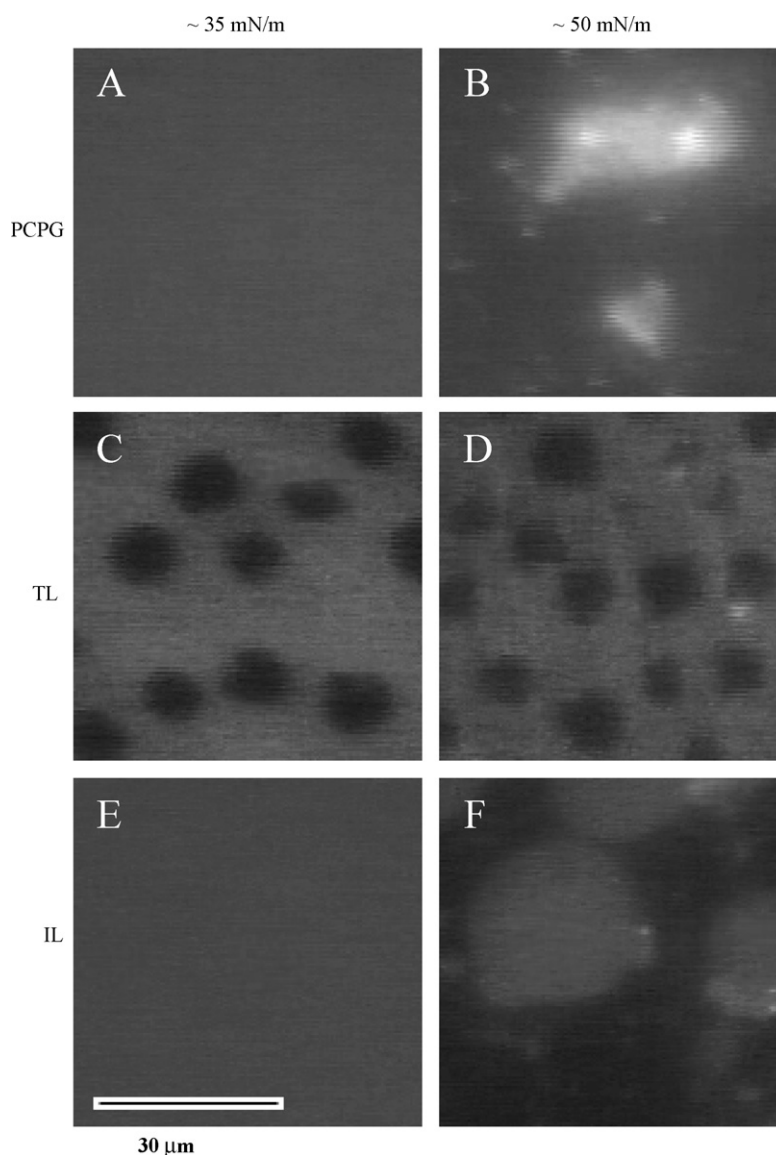


Fig. 2. Fluorescent microscopic images of PCPG lipids (A and B), Tanaka lipids (C and D), and synthetic Infasurf lipids (E and F) at  $\sim 35$  mN/m (A, C and E) and  $\sim 50$  mN/m (B, D and F) on buffer at  $37^\circ\text{C}$ , collected with a barrier speed of 5 mm/min.

with several small vesicles (bright spots) interspersed throughout. The diverse but distinct phase morphologies and variations in bright vesicle size and shape observed in all three lipid formulations at high surface pressure (low-surface tension) indicate that the mechanism through which material is removed from the interfacial lipid layer upon compression is probably different in each case.

#### 3.1.4. Static-bubble pulsating bubble surfactometry results

Static-bubble PBS experiments were performed to observe the kinetics of adsorption of the three surfactant formulations to the air–liquid interface of a bubble. Natural LS is expected to show a rapid decrease in surface tension on the PBS, reaching 25 mN/m within less than 1 min of initial adsorption [38,79]. The hydrophobic surfactant proteins are thought to play a significant role in enabling this fast adsorption. Not unexpectedly, the lipid formulations with no added SP mimics do not adsorb rapidly

to the interface, nor do they reach low equilibrium surface tensions (Fig. 3A). After 20 min of adsorption, PCPG reaches an equilibrium surface tension of  $\sim 55$  mN/m, TL  $\sim 46$  mN/m, and IL  $\sim 55$  mN/m. The lower equilibrium surface tension reached by the TL film versus the PCPG film is likely due to a higher fluidity of the TL film caused by the presence of PA, which occupies a smaller molecular area in the monolayer than DPPC or POPG. The higher surface tension obtained with the IL film may be attributed, in part, to the highly ordered phases that cholesterol induces at low-surface pressures, which can preclude lipid adsorption to the interface in certain regions. Although the role of cholesterol in the surface-active behavior of lipid films is not well understood, it is known to be partially immiscible with phospholipids, depending on the  $T_c$  and the phase of the lipids, and may either fluidize or rigidify the monolayer as a result [80,81]. The overall effect on biophysical activity is still under investigation.

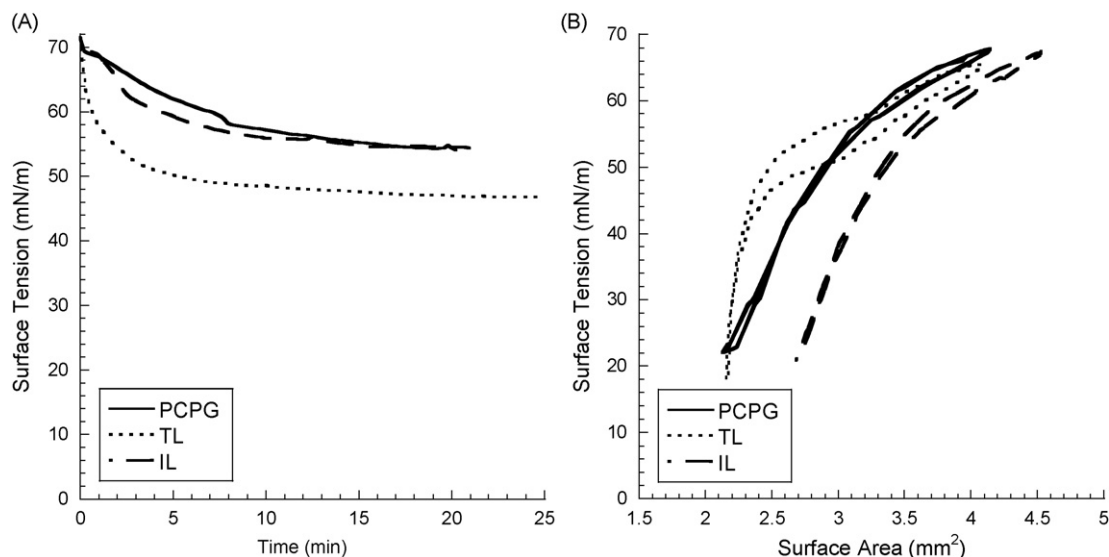


Fig. 3. Static-bubble (A) and dynamic-bubble (B) adsorption results from the pulsating bubble surfactometer in buffer at 37 °C for PCPG lipids, Tanaka lipids, and synthetic Infasurf lipids. Dynamic data were collected at 20 cycles/min and loop directions are clockwise.

### 3.1.5. Dynamic-bubble pulsating bubble surfactometry results

Surface tension ( $\gamma$ ) versus surface area ( $A$ ) data loops may be collected by running the PBS in the dynamic-bubble mode, with a cycling rate similar to that for adult respiration (20 cycles/min). The  $\gamma$ - $A$  loop for natural LS containing SPs is expected to exhibit a maximum surface tension ( $\gamma_{\max}$ ) of about 35 mN/m and a minimum surface tension ( $\gamma_{\min}$ ) near zero, with near-zero surface tension reached after a small amount of compression [38,79]. The  $\gamma$ - $A$  loops obtained using the modified PBS for PCPG, TL, and IL are shown in Fig. 3B. As expected, both  $\gamma_{\max}$  and  $\gamma_{\min}$  for all formulations are significantly higher than what is typically observed for natural LS (with  $\gamma_{\max} \sim 65$  mN/m and  $\gamma_{\min} \sim 20$  mN/m for all three lipid formulations), and do not differ greatly from one another. In addition, we observe no appreciable hysteresis in any of the data loops. Interestingly, although the composition of the PCPG and IL films is drastically different, these loops are nearly identical. Furthermore, the addition of one component (PA) to a PCPG film (*i.e.* the TL film) does result in a slightly lower  $\gamma_{\max}$  and  $\gamma_{\min}$ , and a significantly different loop shape. The slope upon expansion of the TL film is quite steep, indicating that the elasticity of the film is increased with the presence of PA. This is not the case for either the PCPG or IL films, which have substantially lower apparent film elasticities [82].

Though definitive correlations between LWSB and PBS data have not yet been established, it seems that the *in vitro* quasi-equilibrium (LWSB), as well as the adsorptive and dynamic (PBS) surface-active behaviors of all three lipid formulations are similar, with TL film showing the most unique surface-active behavior. The most apparent differences of TL from IL or PCPG in the current *in vitro* testing are in the lipid phase formation and general elasticity and respreadability of the lipid film. However, no specific data would predict poor *in vivo* efficacy in the lung for TL versus IL or PCPG. To further investigate the overall adsorption, respreading, and phase formation of the different

lipid mixtures in an *in vitro* setting, their surface-active behaviors were characterized in the presence of SP-B and SP-C peptide and peptoid mimics using the same *in vitro* techniques.

### 3.2. *In vitro* surface-active behaviors of peptide and peptoid mimics in various lipid formulations

#### 3.2.1. Description of peptoid addition to lipid formulations

To investigate different lipid-lipid and lipid-peptide/peptoid interactions, experiments were performed with SP-B<sub>1-25</sub>, Peptoid B, SP-C<sub>F,F</sub>, or Peptoid C (Table 1) added to each of the three lipid formulations. SP-B<sub>1-25</sub> and SP-C<sub>F,F</sub> were added to each lipid formulation at 10 wt.%, similar to the total protein concentration in LS, while Peptoid B and Peptoid C were added to the lipids at the mole percentage equivalent to 10 wt.% of the respective peptides B and C (Table 2). We have studied the effect of varying the weight percentage of peptoid-based mimics (5%, 10%, and 20%) on the surface activity in a lipid film [83]. We found that at low weight percentages ( $\leq 5\%$ ) the surface activity was inferior relative to 10%, while at high weight percent (20%) there was little change in activity over 10%. Surface activities were investigated using the LWSB, FM imaging, and the PBS. Although many separate features of LWSB and PBS data correlate to the unique behavior and physiological functions of natural LS, it is not yet conclusively known which of these properties are most important for biomedical efficacy. However, it is assumed that a formulation that closely emulates the *in vitro* surface-active behaviors of natural LS is most likely to provide *in vivo* activity that is similar to that of natural LS.

#### 3.2.2. Langmuir–Wilhelmy surface balance results

##### 3.2.2.1. Effect of peptide or peptoid addition to PCPG films.

$\Pi$ - $A$  isotherms obtained at 37 °C reveal that when any of the mimics is added to any one of the lipid formulations, the lift-off area is increased and the resulting plateau (when applicable) is more pronounced (Fig. 4). Similar results are observed at 25 °C



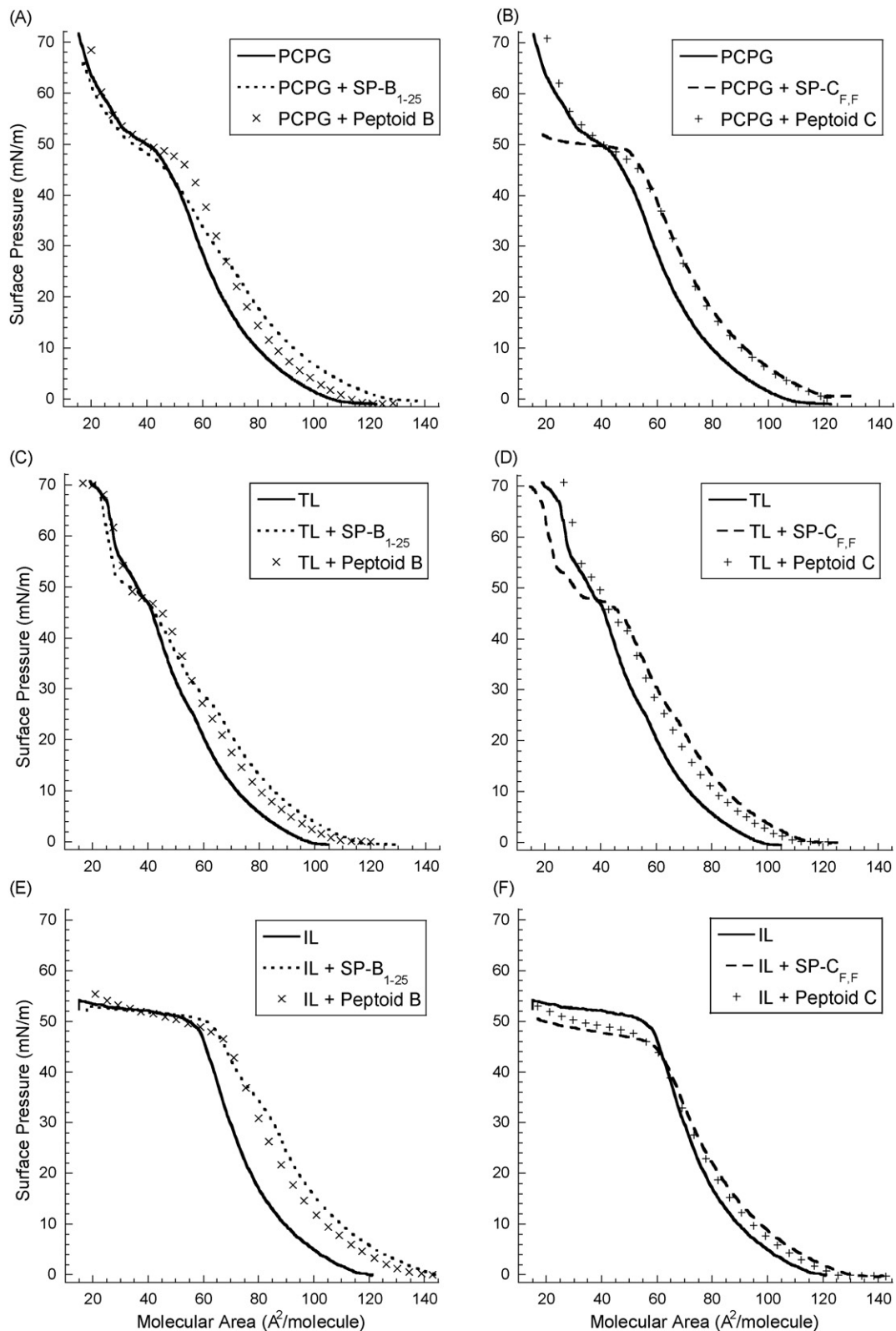


Fig. 4. Surface pressure–surface area isotherms obtained using the Langmuir–Wilhelmy surface balance at 37 °C for PCPG lipids (A and B), Tanaka lipids (C and D), and synthetic Infasurf lipids (E and F) with added SP-B (A, C and E) or SP-C mimics (B, D and F). Molecular areas include both lipids and mimics.

(data not shown). An increase in lift-off area is expected for lipid formulations containing additional peptide or peptoid, as additives alter the available area per molecule, and presumably, the presence of surface-active SP mimics facilitates lipid–lipid

and lipid–peptide/peptoid interactions, causing increased film organization and a subsequent surface pressure increase at a larger molecular area relative to the lipid mixture without added spreading agents. Since a plateau in the isotherm is thought to

correspond to structural reorganization and material removal from the interface, a more pronounced plateau is considered desirable, as it mimics that of the natural LS film.

For the PCPG film at 37 °C (lift-off area  $\sim 107 \text{ \AA}^2/\text{molecule}$ ), the addition of the SP-B<sub>1–25</sub> peptide increases the lift-off area to  $\sim 130 \text{ \AA}^2/\text{molecule}$ , while the addition of Peptoid B increased the lift-off area to  $\sim 115 \text{ \AA}^2/\text{molecule}$  (Fig. 4A). We also observe an increase in lift-off area, to  $\sim 120 \text{ \AA}^2/\text{molecule}$  (Fig. 4B) upon the addition of SP-C<sub>FF</sub> and Peptoid C. Strikingly, the addition of the SP-C<sub>FF</sub> peptide to PCPG results in a low film collapse pressure of  $\sim 50 \text{ mN/m}$ , indicating that the film does not undergo the LC to solid phase transition. On the other hand, the film containing SP-B<sub>1–25</sub> exhibits a higher lift-off area than the other SP mimic-containing films, which may be due to its occupation of a larger area at the interface (though SP-C<sub>FF</sub> peptide is longer and presumably larger, likely has a greater tendency to associate with lipid acyl chains and orient transversely or angle into the monolayer), and/or SP-B<sub>1–25</sub>'s increased ability to organize a lipid film and promote molecular interactions in the 2D gas–liquid coexistence phase at a larger molecular area relative to the other mimics. The addition of Peptoid B to the PCPG film, on the other hand, results in a more pronounced plateau between 45 and 50 mN/m compared to the other mimics, indicating an increased degree of structural reorganization or facilitated removal of material from the monolayer in this range of surface pressures.

**3.2.2.2. Effect of peptide or peptoid addition to TL films.** In the TL film, SP-B<sub>1–25</sub> exhibits a lift-off area of  $\sim 115 \text{ \AA}^2/\text{molecule}$ , while Peptoid B exhibits a lift-off area of  $\sim 110 \text{ \AA}^2/\text{molecule}$ , while SP-C<sub>FF</sub> exhibits a lift-off area of  $\sim 120 \text{ \AA}^2/\text{molecule}$ , and Peptoid C exhibits a lift-off area of  $\sim 115 \text{ \AA}^2/\text{molecule}$ , versus  $\sim 100 \text{ \AA}^2/\text{molecule}$  for the TL film without any additives (Fig. 4C and D). The significant changes in lift-off area for peptides and peptoids in TL relative to the PCPG lipid mixture indicate that the area occupied by the added surface-active SP mimics at the interface is not the sole determinant for the increased lift-off area values. In all instances, the collapse pressure for the TL formulations is high ( $\sim 70 \text{ mN/m}$ ) and a kink or plateau is observed between 45 and 50 mN/m, with more pronounced plateaus for the films with added SP-B<sub>1–25</sub>, Peptoid B, or SP-C<sub>FF</sub>. Interestingly, the extent of the plateau for TL films containing SP-B<sub>1–25</sub> or Peptoid B are quite similar to each other, in contrast to those in the PCPG films. In addition, SP-C<sub>FF</sub> in the TL film is able to reach collapse at a high surface pressure, though there is only one lipid component difference between the TL and PCPG films (PA). Specific, electrostatic interactions between anionic PA and the cationic residues at positions 11 and 12 in SP-C<sub>FF</sub> may play a role in stabilizing the film at higher surface pressures. In reaching a higher collapse pressure, an extended plateau region is observed, which is significantly different from all other plateau regions presented here. Amongst the TL films, those containing either SP-B<sub>1–25</sub> or SP-C<sub>FF</sub> exhibit slightly earlier lift-off areas and more pronounced plateaus than the films containing the peptoid-based mimics, indicating overall better surface activities for the peptides, although the differences overall are relatively small.

**3.2.2.3. Effect of peptide or peptoid addition to IL films.** The lift-off area for the IL film is increased with the addition of all SP mimics (to  $\sim 145 \text{ \AA}^2/\text{molecule}$  for SP-B<sub>1–25</sub> and Peptoid B,  $\sim 135 \text{ \AA}^2/\text{molecule}$  for SP-C<sub>FF</sub>, and  $\sim 130 \text{ \AA}^2/\text{molecule}$  for Peptoid C (Fig. 4E and F)). These lift-off areas are significantly higher than those observed for either the PCPG or TL films, probably due to the higher concentrations of unsaturated lipids with bulky tails. It is again observed here, as in the PCPG and TL films, that the presence of a peptide SP mimic results in a slightly higher lift-off area than the presence of a peptoid SP mimic. However, as with the IL-only films, the IL films in the presence of SP mimics are still unable to reach high surface pressures, with a collapse pressure that is significantly lower ( $\sim 50 \text{ mN/m}$ ), indicating that these films do not form stable LC phases. As previously mentioned, this early collapse is likely due to the tendency of cholesterol to create disordered, fluid phases at higher surface pressures [72]. As a result, all of the formulations exhibit extended plateau regions until the point of film collapse, at  $\sim 50 \text{ mN/m}$ . In the IL films, SP-B<sub>1–25</sub> again exhibits a somewhat earlier lift-off area than the other mimics, as well as an extra kink in the isotherm at 30–40 mN/m, indicating that this peptide has moderately greater surface activity than the other mimics.

### 3.2.3. FM imaging results

To gain further insight into lipid phase transitions and general phase morphology, FM images were captured for these lipid–peptide/peptoid films. In Fig. 5, FM images are shown for PCPG alone (A and B) and with added SP-B<sub>1–25</sub> (C and D), Peptoid B (E and F), SP-C<sub>FF</sub> (G and H), or Peptoid C (I and J) at 37 °C from before the plateau,  $\sim 35 \text{ mN/m}$  (A, C, E, G and I), and during the plateau,  $\sim 50 \text{ mN/m}$  (B, D, F, H and J). FM images for TL and IL films without and with added mimics are similarly shown in Figs. 6 and 7, respectively (panels labeled as described above). At  $\sim 35 \text{ mN/m}$ , no LC domain formation is observed for any of the PCPG or IL formulations with the added SP mimics, while dark LC domains are observed for all of the TL formulations, as was observed for the lipid-only films (Fig. 2). For PCPG and IL films, the addition of peptide or peptoid does not induce observable phase separation at this lower surface pressure. For TL films, both the size and spacing of the domains are similar for all of the films except that containing Peptoid C, which shows significantly smaller LC domains and a slightly tighter packing density. Thus, Peptoid C is able to affect lipid domain packing and density at lower surface pressures when compared to the other mimics, which is an indication of increased surface activity.

At  $\sim 50 \text{ mN/m}$ , domain formation is observed for all of the films. Bright domains, indicative of vesicle formation, are observed for all of the PCPG films (Fig. 5). The addition of SP-B<sub>1–25</sub> or Peptoid B to PCPG results in the formation of large, bright circular domains, with the SP-B<sub>1–25</sub>-containing film having very large domains. These types of domains are indicative of vesicle formation below the monolayer, which may point to a specific mechanism of material removal from the monolayer and submonolayer organization for each of these SP mimics [75]. The addition of SP-C<sub>FF</sub> or Peptoid C also results in the

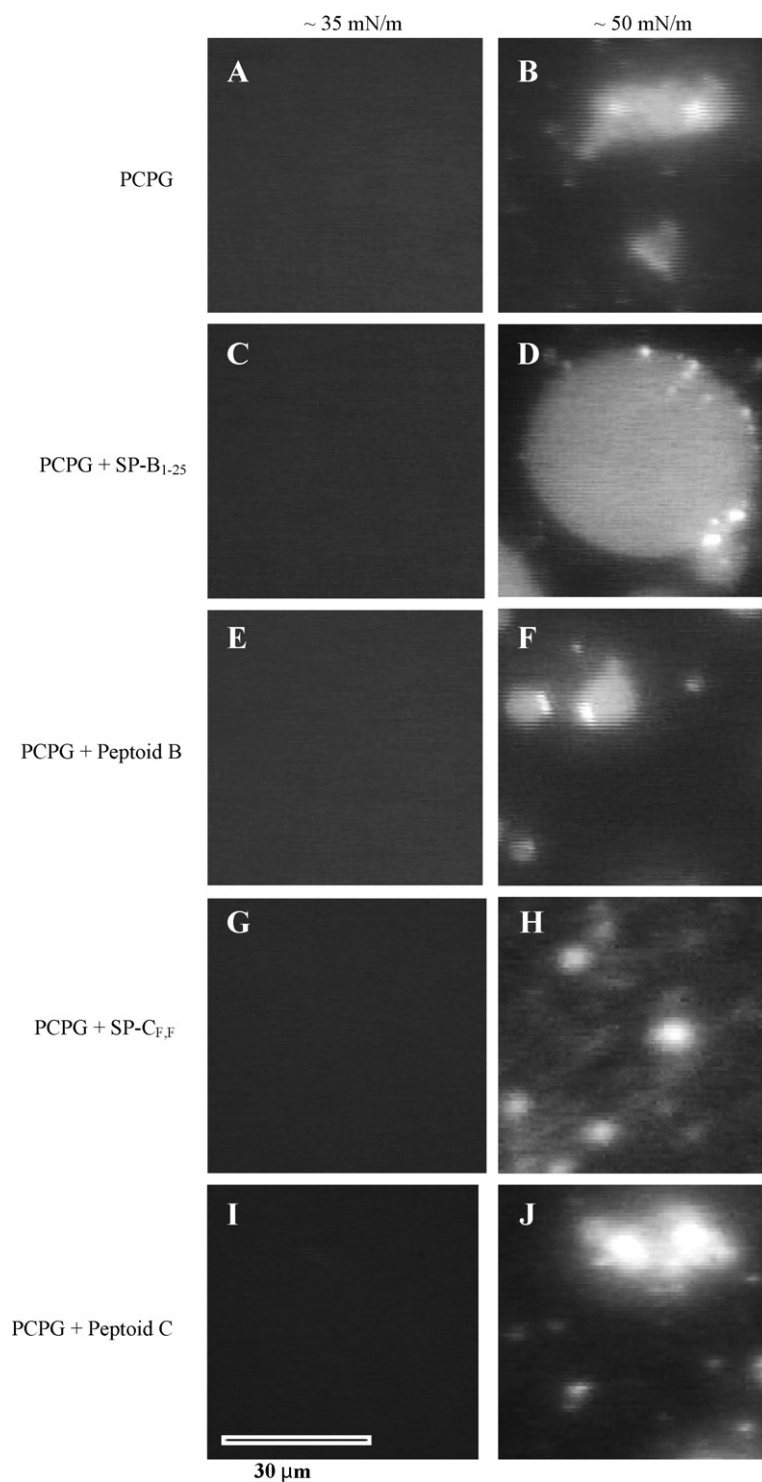


Fig. 5. Fluorescent microscopic images for PCPG lipids (A and B), PCPG lipids with added SP-B<sub>1-25</sub> (C and D), Peptoid B (E and F), SP-C<sub>F,F</sub> (G and H), and Peptoid C (I and J) on buffer at 37 °C, collected with a barrier speed of 5 mm/min. Images shown for  $\Pi \sim 35$  mN/m (A, C, E, G and I) and  $\Pi \sim 50$  mN/m (B, D, F, H and J).

formation of bright vesicles; however, the observed domains are more numerous and display a different morphology from those seen in SP-B<sub>1-25</sub>- and Peptoid B-containing films. Note that although the PCPG film with Peptoid C was unable to reach collapse at a high surface pressure, the type of vesicle formation observed here is very similar to that of PCPG + SP-C<sub>F,F</sub> (Fig. 5H

and J). At  $\sim 50$  mN/m dark LC domains are still observed for the TL films, although they may not be discernable in the presented FM images (Fig. 6). However, for those films containing SP mimics, scattered small, bright vesicles are also observed. The SP-B<sub>1-25</sub>-containing film has very few vesicles, while the films containing Peptoid B and Peptoid C exhibit significantly

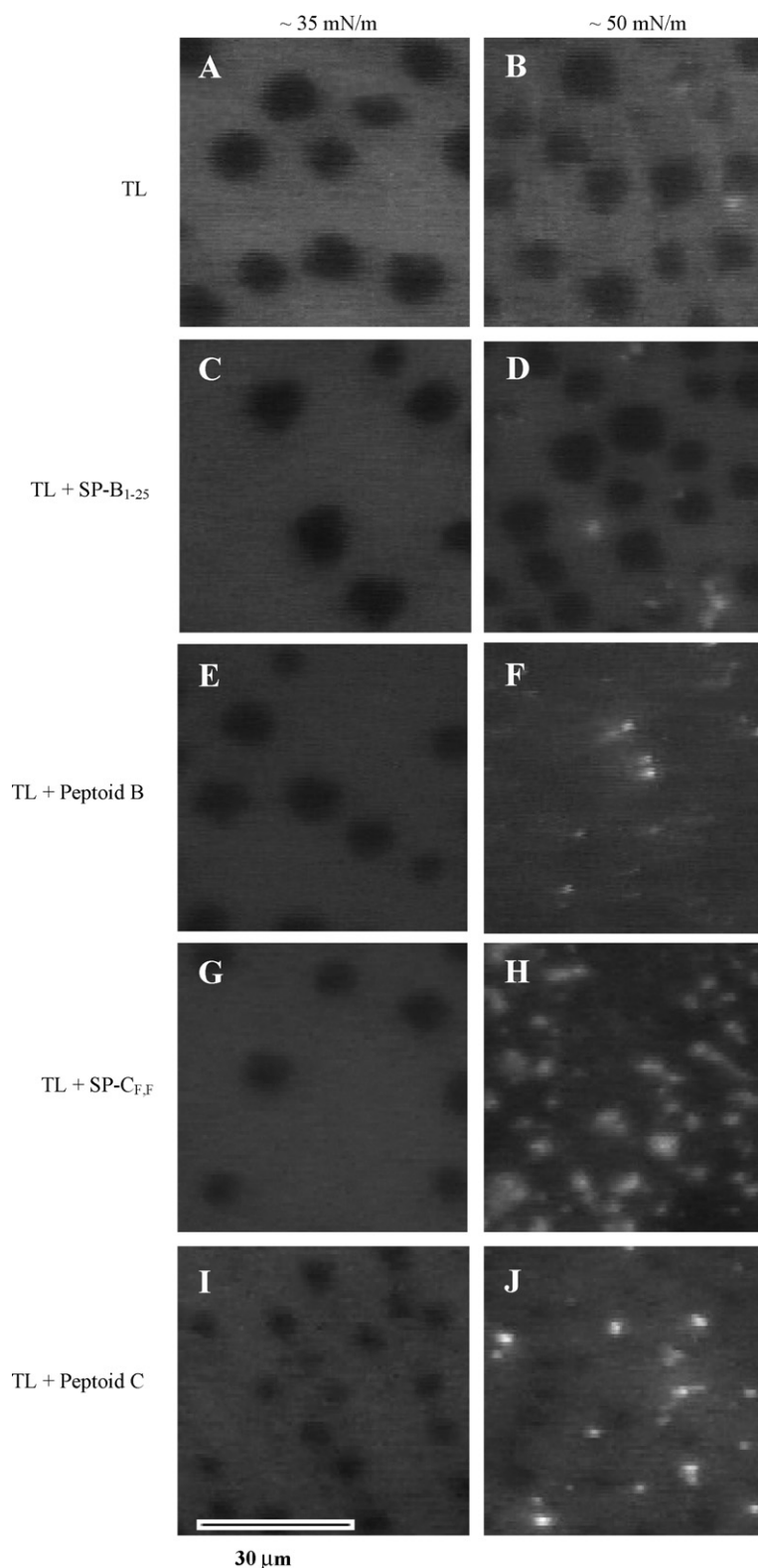


Fig. 6. Fluorescent microscopic images for Tanaka lipids (A and B), Tanaka lipids with added SP-B<sub>1-25</sub> (C and D), Peptoid B (E and F), SP-C<sub>FF</sub> (G and H), and Peptoid C (I and J) on buffer at 37 °C, collected with a barrier speed of 5 mm/min. Images shown for  $\dot{\Gamma} \sim 35$  mN/m (A, C, E, G and I) and  $\dot{\Gamma} \sim 50$  mN/m (B, D, F, H and J).

more and SP-C<sub>FF</sub> shows an even larger number, making it difficult to observe the dark LC domains. Note that the formation of very large vesicle domains is not observed in any TL films. The IL films possess phase morphology very similar to that of

PCPG, where bright vesicle domains are observed at  $\sim 50$  mN/m (Fig. 7). The IL film containing SP-B<sub>1-25</sub> exhibits very large, bright domains, while that containing Peptoid B has medium-sized bright domains interspersed with small bright vesicles.

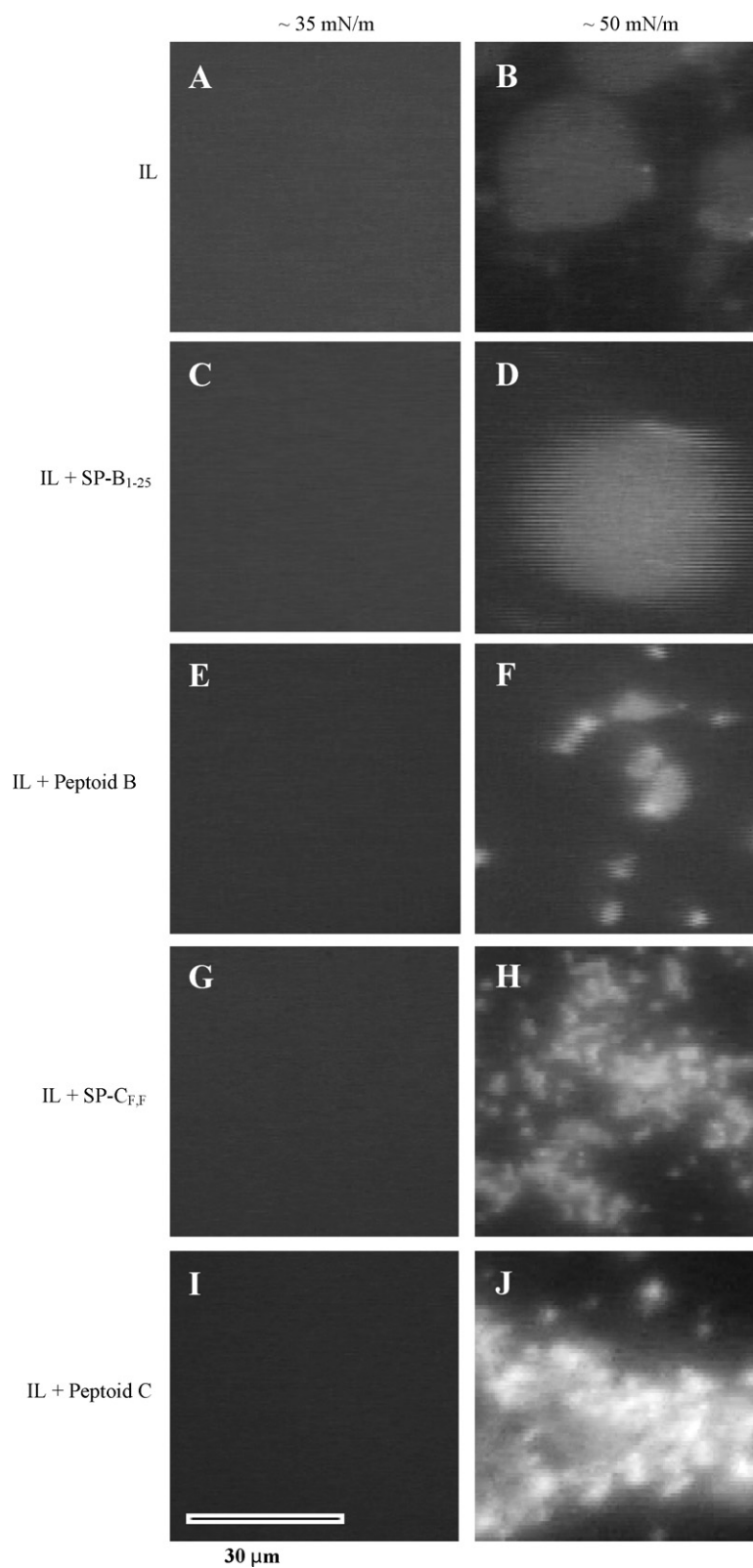


Fig. 7. Fluorescent microscopic images for synthetic Infasurf lipids (A and B), synthetic Infasurf lipids with added SP-B<sub>1-25</sub> (C and D), Peptoid B (E and F), SP-C<sub>F,F</sub> (G and H), and Peptoid C (I and J) on buffer at 37 °C, collected with a barrier speed of 5 mm/min. Images shown for  $\Pi \sim 35 \text{ mN/m}$  (A, C, E, G and I) and  $\Pi \sim 50 \text{ mN/m}$  (B, D, F, H and J).

Finally, the SP-C mimic-containing films show large numbers of small bright vesicles.

Overall, the size, shape, and degree of vesicle formation at higher surface pressures for SP-B versus SP-C mimics are quite distinguishable. While SP-B<sub>1–25</sub> or Peptoid B promote the formation of medium to large, or in the case of SP-B<sub>1–25</sub>, very large, bright vesicular domains in PCPG and IL films, the presence of SP-C<sub>F,F</sub> or Peptoid C in these films tends to result in numerous, smaller, bright vesicular domains. As SP-C has often been pointed to as the protein that anchors lipids to the interface for easy incorporation upon film area expansion, it would be logical to hypothesize that it facilitates the formation of smaller vesicle domains for this reason. In general, the significance of the size, shape, and degree of vesicles formed during compression has not been extensively investigated, although their presence is the obvious result of lipid–lipid and lipid–peptide/peptoid interactions and overall structural reorganization at the interface as surface pressure increases and available film area becomes smaller [71].

Also notable is that, of the three lipid formulations, TL in the presence of any SP mimics consistently produces smaller bright domains when compared to the PCPG or IL mixtures. If vesicle domain size correlates inversely with enhanced elasticity or respreadability, we would predict that TL (the most elastic of the films) would produce smaller domains independent of the presence of SP mimics, which is what we observe. This phenomenon could explain why TL has up to this point been considered a very good *in vitro* mimic of the non-protein portion of LS, despite its reportedly poorer *in vivo* efficacy.

### 3.2.4. Static-bubble pulsating bubble surfactometry results

Static-bubble adsorption data collected using the PBS reveal a substantial increase in the surfactant adsorption rate and an enormous decrease in equilibrium surface tension values reached with the addition of SP mimics to any of the lipid formulations (Fig. 8). In a PCPG film (panels A and B), SP-B<sub>1–25</sub> facilitates the attainment of a low equilibrium surface tension of  $\sim 20$  mN/m after approximately 7 min, while the film containing Peptoid B only reaches an equilibrium surface tension of  $\sim 30$  mN/m after approximately 15 min, indicating more rapid adsorption to the interface for SP-B<sub>1–25</sub>- than Peptoid B-containing PCPG films. Much more rapid adsorption to the interface is observed for SP-C<sub>F,F</sub> films, with an equilibrium surface tension of  $\sim 25$  mN/m reached in less than 1 min. Peptoid C films also reach an equilibrium surface tension of  $\sim 25$  mN/m, but like SP-B<sub>1–25</sub>- and Peptoid B-containing films, require nearly 10 min, for complete adsorption. The greater number of hydrophobic amino acids in the peptide-based SP mimics (relative to the shorter peptoids) may contribute to the faster adsorption kinetics observed with the peptide-containing films relative to those of the peptoid-containing films.

In TL (panels C and D), films containing either SP-C<sub>F,F</sub> or Peptoid C reach the low equilibrium surface tension of  $\sim 25$  mN/m seen in PCPG films very rapidly, after only about 2 min. Peptoid B films also reach an equilibrium surface tension of  $\sim 25$  mN/m, but require about 5 min to adsorb. Films

containing SP-B<sub>1–25</sub> only reach a surface tension of  $\sim 30$  mN/m after about 7 min. In IL (panels E and F), films containing SP-C<sub>F,F</sub> and Peptoid C again reached the desirably low equilibrium surface tension of  $\sim 25$  mN/m, with an adsorption time of less than a minute for SP-C<sub>F,F</sub> and about 2 min for Peptoid C. SP-B<sub>1–25</sub> and Peptoid B films also reach an equilibrium surface tension of  $\sim 25$  mN/m, but require more time to adsorb ( $\sim 7$  min for SP-B<sub>1–25</sub> and  $\sim 13$  min for Peptoid B).

Therefore, the presence of SP mimics in all lipid films greatly reduces the equilibrium surface tensions reached during adsorption, to nearly that of natural LS ( $\sim 25$  mN/m). The values reached are consistent for SP-C mimics, but vary for SP-B mimics, depending on the lipid composition of the film. For instance, SP-B<sub>1–25</sub> only reaches 30 mN/m in TL films, but can bring the surface tension down to 20 mN/m in PCPG films. An opposite trend is seen for Peptoid B, which reaches 30 mN/m in PCPG films, but attains 25 mN/m in TL films. Also worth noting is that the rate of adsorption for SP-B mimics is consistently quite slow compared to SP-C mimics. SP-C mimics may be able to interact more readily with the lipids than SP-B mimics due to their greater hydrophobicity, promoting a drastic increase in the rate of adsorption. It is intriguing that though the respective equilibrium surface tensions reached for the different lipid films in the presence of each SP mimic are nearly the same, the rates of adsorption vary tremendously. These results point to the importance of carefully selecting both a good synthetic lipid mixture and good SP mimics (appropriately paired) for *in vivo* and *in vitro* testing. Overall, the *in vitro* performance of the TL formulation is best for the SP mimics studied based on these static-bubble adsorption data.

### 3.2.5. Dynamic-bubble results

Dynamic-bubble PBS experiments also reveal a substantial increase in biomimetic surfactant activity with added SP mimics as expected, but the differences between the formulations are quite significant once again (Fig. 9). For all SP mimic-containing films, a decrease in the maximum surface tension ( $\gamma_{\max}$ ) and an increase in data loop hysteresis are observed. However, the  $\gamma_{\max}$  reached by films containing peptide-based mimics are significantly lower than for films containing peptoid-based mimics. In PCPG films (Fig. 9A and B), only the addition of SP-B<sub>1–25</sub> facilitates a decrease in  $\gamma_{\min}$ , from  $\sim 20$  to  $\sim 10$  mN/m, with a slight increase in hysteresis at high surface areas also observed. An increase in hysteresis at low-surface areas is observed for films containing Peptoid B or SP-C<sub>F,F</sub>. High hysteresis at low-surface tension corresponds to an ability to reach low-surface tension with only a small amount of film area compression, similar to LS. Interestingly, Peptoid C-containing PCPG films show only a slight decrease in  $\gamma_{\max}$  and very little increase in hysteresis at low-surface tensions, and otherwise the shape of the data loop is very similar to the PCPG film containing no additives. This indicates that Peptoid C is not significantly enhancing the dynamic surface activity of this lipid film, which is surprising considering the experimental findings obtained with the LWSB and FM, as well as the static PBS results. Here, the overall dynamic *in vitro* performance of all the PCPG films is poor; films do not reach near-zero surface tensions upon compression with peptoids or

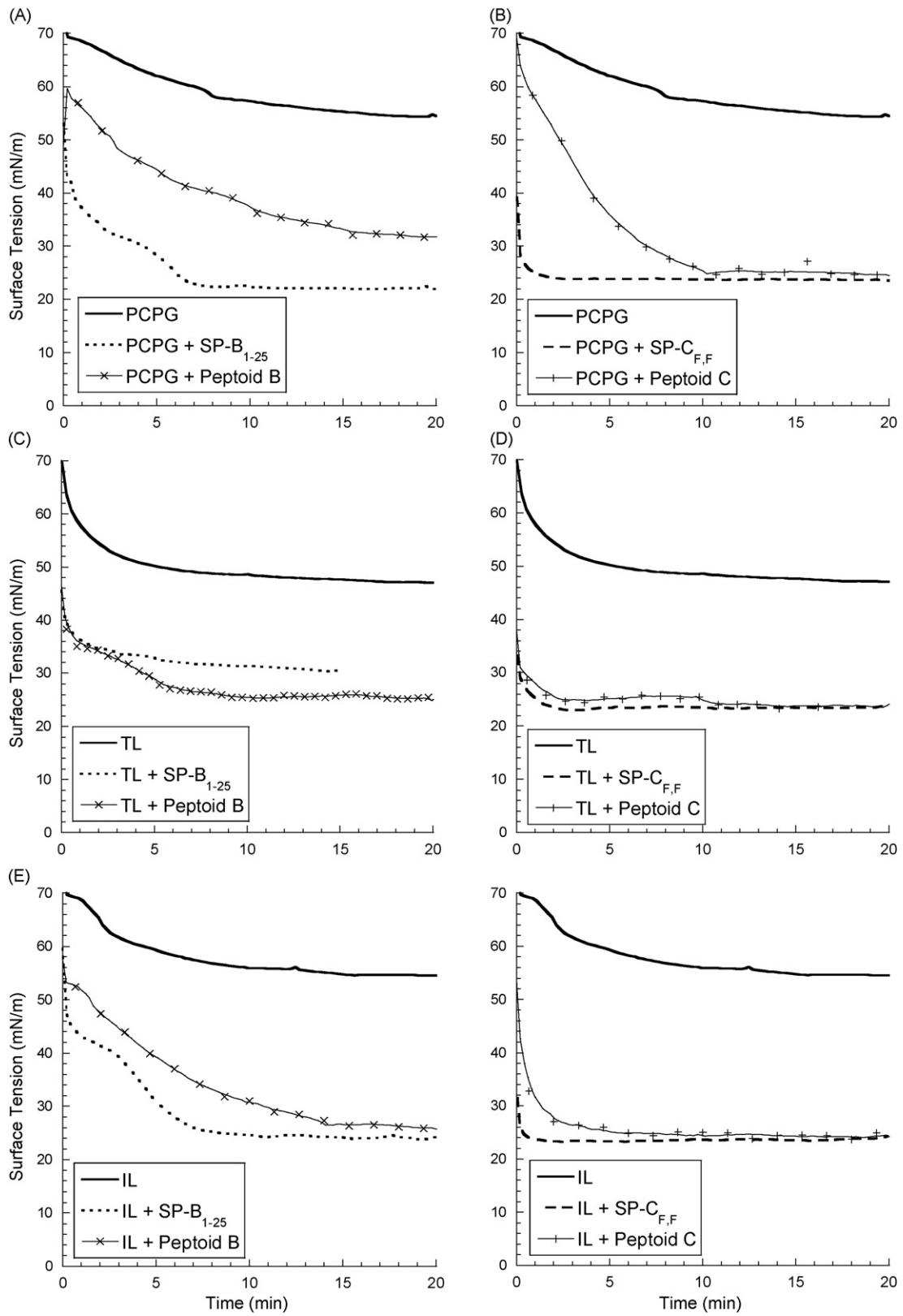


Fig. 8. Static-bubble adsorption results from the pulsating bubble surfactometer in buffer at 37 °C for PCPG lipids (A and B), Tanaka lipids (C and D), and synthetic Infasurf lipids (E and F) with added SP-B (A, C and E) or SP-C mimics (B, D and F).

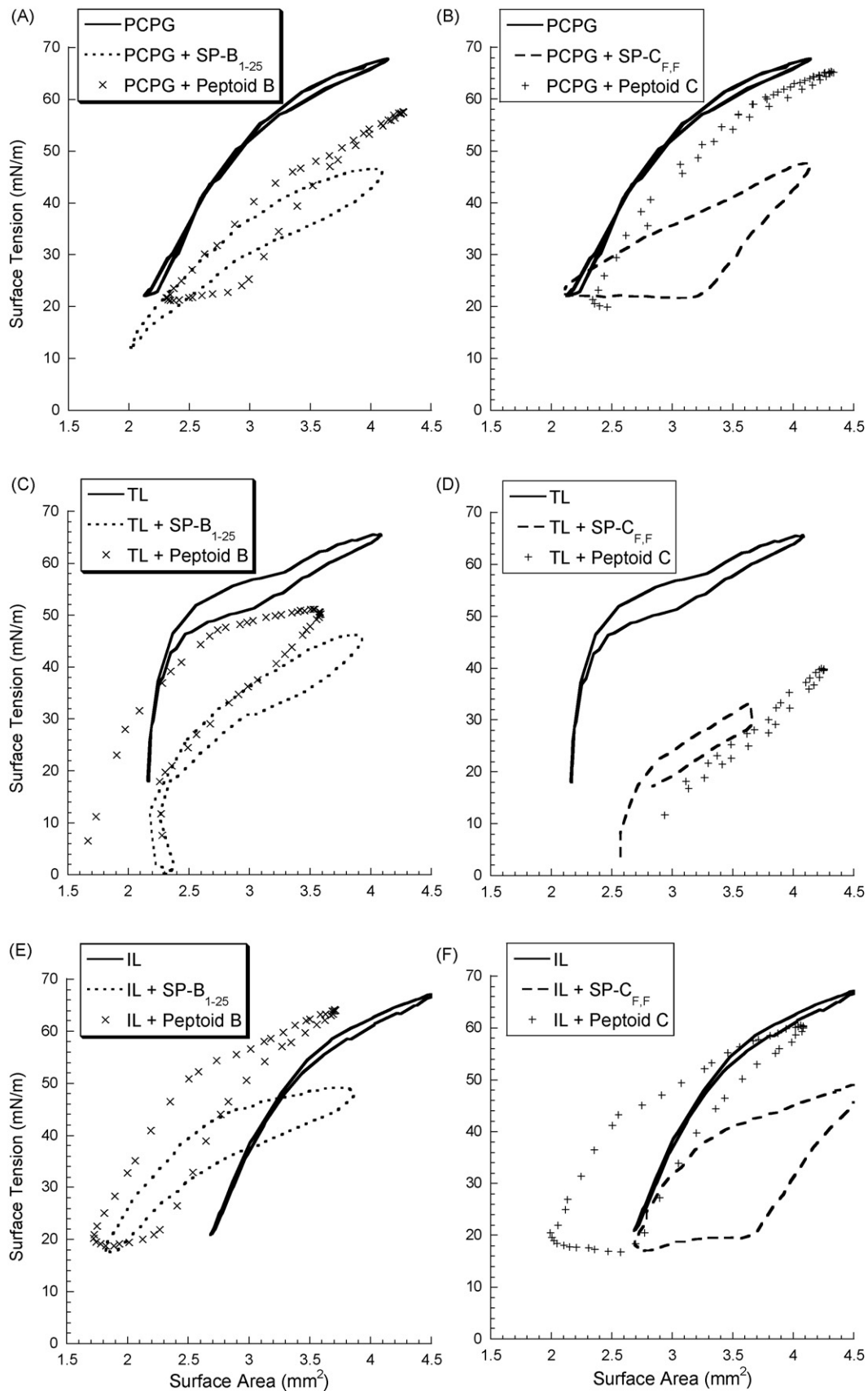


Fig. 9. Dynamic-bubble adsorption results from the pulsating bubble surfactometer in buffer at 37 °C for PCPG lipids (A and B), Tanaka lipids (C and D), and synthetic Infasurf lipids (E and F) with added SP-B (A, C and E) or SP-C mimics (B, D and F). Data were collected at 20 cycles/min and loop directions are clockwise.



with peptides that are known to mimic the native proteins fairly well.

The shape of the bubble loop significantly changes for all mimics in TL films as compared to PCPG films. In TL films (Fig. 9C and D),  $\gamma_{\max}$  is reduced to  $\sim 45$  mN/m with added SP-B<sub>1–25</sub>,  $\gamma_{\max} \sim 50$  mN/m with added Peptoid B,  $\gamma_{\max} \sim 32$  mN/m with added SP-C<sub>F,F</sub>, and  $\gamma_{\max} \sim 40$  mN/m with added Peptoid C, as compared to  $\sim 65$  mN/m for the pure lipid film. Interestingly, the SP-C mimics are clearly able to reduce  $\gamma_{\max}$ , and considerably more so than the SP-B mimics. Peptoid C, which in PCPG films failed to enhance surface activity when compared to pure PCPG, shows a dramatic increase in surface activity in TL films, with  $\gamma_{\max}$  values significantly lower than for all mimics but SP-C<sub>F,F</sub>. Again, the PA component appears to have the pronounced effect of improving the surface activity of TL in the presence of SP-C mimics, relative to the surface activity of the mimics in PCPG films without PA. Additionally, the  $\gamma_{\min}$  is decreased to nearly zero (as is desirable) for all SP mimic-containing TL films. Note that since for these formulations bubble shape greatly deforms from that of an ellipse at near-zero surface tensions, the image analysis system is not able to track a symmetrical bubble shape and we are not able to calculate the surface area nor surface tension of the bubble. However, it is clear that near-zero surface tensions are obtained in these instances because the pressure drop is very low and the bubble shapes are highly deformed. Note however that these low-surface tension data points are not shown on the plots; these low- $\gamma$  data were omitted from the dynamic PBS plots for both TL/Peptoid B films (Fig. 9C) and TL/SP-C<sub>F,F</sub> and TL/Peptoid C films (Fig. 9D). While a slight increase in data loop hysteresis is observed for films containing SP-B<sub>1–25</sub>, SP-C<sub>F,F</sub>, and Peptoid C, a relatively large extent of hysteresis is observed for Peptoid B films, which is generally thought to be a good biomimetic feature.

In IL formulations (Fig. 9E and F),  $\gamma_{\max}$  is decreased and hysteresis is increased with added SP mimics, while  $\gamma_{\min}$  remains approximately the same as the lipid-only film at  $\sim 20$  mN/m. Similar to the PCPG and TL films,  $\gamma_{\max}$  is decreased to a greater extent with added peptide mimics ( $\sim 45$  mN/m) than peptoid mimics ( $\sim 60$  mN/m). Films containing Peptoid B, SP-C<sub>F,F</sub>, or Peptoid C all show increased hysteresis at both high and low-surface areas, while SP-B<sub>1–25</sub> films only show greatly increased hysteresis at high surface areas. However, like PCPG films, all IL films fail to reach the near-zero surface tensions considered critical for efficacy of an LS formulation.

Based on the dynamic-bubble PBS results, it appears that only TL formulations with added SP mimics are able to reach near-zero minimum surface tensions upon film compression. However, IL formulations with added SP mimics tend to have a greater amount of hysteresis than the TL formulations (especially for those containing the SP-C analogues), which is considered desirable in an LS formulation. The main difference between these lipid formulations is that TL contains PA and IL contains cholesterol. To greater elucidate the role and importance of these two different surfactant components, we designed five additional lipid formulations, in which cholesterol was either excluded from, or PA added to, the IL formulation. No significant differences in the minimum surface tensions nor

the extent of hysteresis in the PBS data loops were observed for these variant IL lipid formulations in combination with Peptoid B (data not shown). Hence, these compositional differences do not appear to be exclusively responsible for the unusual behavior of IL-based films. It could also be reasoned that the difference in unsaturated phospholipid content among the formulations influenced the amount of compression required to reach minimum surface tensions in the presence of SP mimics. IL has significantly higher unsaturated phospholipid content than either PCPG or TL, and the increased extent of lipid acyl chain interactions with SP mimics may promote more rapid changes in surface tension with small amounts of compression.

### 3.2.6. Notes on the surface-active behavior of DPPC-containing films at low-surface tensions

Very recent work by Gopal and Lee [84] has lent valuable insight into the collapse and low-surface tension behaviors of DPPC-containing mixed lipid monolayers, which may be applied to the current investigation. Through the study of Langmuir isotherms and 2D bulk moduli of DPPC:PA and DPPC:DMPA mixtures with increasing mole fractions of DPPC ( $\chi_{\text{DPPC}}$ ) at 30 °C, it was determined that a sudden transition in collapse pressure (from 50 to 65 mN/m to 70+ mN/m) occurs in the range of 0.6–0.8  $\chi_{\text{DPPC}}$ , before which, the collapse pressures were  $<60$  mN/m. These data were further compared to that of DPPC:POPG:PA (TL) and DPPC:cholesterol mixtures, and very similar trends were observed [37,84,85]. A simple rigidity percolation treatment argument was applied to explain this phenomenon, and a quantitative explanation for the ‘coincidental’ widespread empirical use of 70% DPPC in LS replacement formulations for *in vitro* use was provided. Based on the  $\chi_{\text{DPPC}}$  of the three lipid mixtures studied here (0.71  $\chi_{\text{DPPC}}$  for PCPG, 0.60  $\chi_{\text{DPPC}}$  for TL, and 0.46  $\chi_{\text{DPPC}}$  for IL), the differences in collapse pressures on the LWSB may now be clearly explained. The  $\chi_{\text{DPPC}}$  in IL (which also contains cholesterol) is lower than the ‘key’ range of 0.6–0.8  $\chi_{\text{DPPC}}$ , and therefore, we observe low collapse pressures ( $\sim 55$  mN/m) in all IL-containing LWSB isotherms at higher temperature. As both PCPG and TL films are above the 0.6  $\chi_{\text{DPPC}}$  threshold for DPPC-containing lipid mixtures, collapse pressures  $>70$  mN/m ( $\sim 2$  mN/m surface tension) are reached. These results clearly support the work of Gopal and Lee. However, all three lipid formulations exhibit significantly elevated minimum surface tensions on the dynamic-bubble PBS ( $\sim 20$  mN/m), where a monolayer-only system no longer exists. Surprisingly, only the TL formulation reaches near-zero surface tensions in the presence of SP mimics on the PBS. As the low-surface tension/high surface pressure regime is believed to be of critical importance in designing and testing LS replacements containing SPs or their mimics, these differences in the interfacial behaviors of mono- versus multilayer DPPC-containing lipid films will continue to be explored.

## 4. Conclusions

Previous work has shown that the addition of either Peptoid B or Peptoid C to TL improves the surface-active behavior of the LS replacement relative to what is observed for the lipids

alone, and that both peptoid-based SP mimics show surface activities in TL that are similar to or in some ways better than that of their respective peptide analogues [26,27]. Although peptoid-containing surfactant film properties compared well with those exhibited by the TL/peptide formulations, they are so far unable to achieve the exact performance exhibited by natural LS [38,79]. In particular, dynamic-bubble PBS experiments revealed that the TL/Peptoid B formulation was able to reach near-zero  $\gamma_{\min}$ , but that  $\gamma_{\max}$  was significantly higher than the 35 mN/m expected for natural LS [26]. In order to create a fully functional, synthetic LS replacement, the optimal lipid formulation must be further investigated; and most likely, better SP mimics will also need to be created.

In this paper we have investigated the *in vitro* surface behavior of peptide- and peptoid-based SP mimics in combination with three commonly used LS-mimetic lipid formulations: PCPG, TL, and IL. These lipid formulations are composed of different types of lipids, allowing the investigation of lipid–lipid and SP mimic/lipid interactions. Among the three lipid formulations, significantly different surface activities were observed. Although the lipid mixtures themselves do not exhibit drastic differences on the PBS, there are significant differences in the LWSB isotherms and FM images at higher surface pressures. The inability of the IL film to sustain high surface pressure/low-surface tension at higher temperature would clearly inhibit us from obtaining information about added SP mimics in this region, which is non-ideal given that surface-active behavior in the low-surface tension regime is considered critical for assessing *in vitro* efficacy. Additionally, although the film phase formation observed in this study *via* FM is not conclusively understood, the presence of dark LC domains in the TL film clearly sets its phase behavior apart from the other lipid mixtures. Previous work in our group has demonstrated that the average domain sizes change depending on the peptoid or peptide added, which may give indications regarding increased surface activity. The effect of this phase morphology on *in vivo* studies has not been definitively assessed, although TL has been reported to have overall poorer *in vivo* efficacy relative to the IL mixture [34].

Additionally, these studies have shown that lipid composition markedly affects the *in vitro* surface activities of the SP mimics added to the formulations. Specifically, combination of SP mimics with all lipid films results in a significantly higher lift-off. However, the PCPG and IL films are not always able to reach the desired high collapse pressures. While TL films form LC domains at both  $\sim 35$  and  $\sim 50$  mN/m, FM imaging of PCPG or IL films reveals no domain formation at  $\sim 35$  mN/m and only vesicle formation at  $\sim 50$  mN/m. Static-bubble PBS results indicate that though equilibrium surface tensions are similar for all lipid films with added mimics, the rate of adsorption can vary tremendously depending on lipid composition. Finally, dynamic-bubble PBS results show that SP mimics in PCPG or IL films are not able to reach near-zero minimum surface tensions, while SP mimics in TL films are. However, IL films in particular are able to reach a minimum surface tension after a small amount of compression. Further investigation of lipid formulations containing varying amounts of cholesterol or PA in

the IL film revealed little effect on the amount of hysteresis and the minimum surface tension.

None of these SP mimic/lipid formulations are able to precisely emulate the surface-active behavior of natural LS, however the TL formulation appears to be most promising for continued *in vitro* study and this is particularly the case for the peptoid-based SP mimics under development in our lab. While a more complex lipid formulation based on the lipid composition of Infasurf<sup>TM</sup> also showed some promising aspects, even with added SP mimics the collapse surface pressure as observed by LWSB is quite low ( $\sim 50$  mN/m) and the minimum surface tension as observed by dynamic-bubble PBS experiments is quite high ( $\sim 20$  mN/m). In terms of biomimetic characteristics, which must be seen with *in vitro* testing in order to assess the functioning of added SP mimics, the TL lipid mixture is the only one to satisfy the requirement of reaching low dynamic surface tensions on both the LWSB and the PBS. Further experiments will be performed using *in vivo* animal models of RDS to study the efficacy of these formulations, and to shed further light on the relationship between these types of *in vitro* observations of surfactant behavior and the physiological functioning of surfactant replacements for the treatment of respiratory distress syndrome.

## Acknowledgements

We thank Dr. Mark Johnson and Dr. Ronald N. Zuckermann for their assistance. This work was supported by the National Science Foundation (Grant nos. BES-9870386 and BES-0101195) and the National Institutes of Health (Grant no. 1R01HL67984-01).

## References

- [1] S.E. Poynter, A.M. LeVine, *Crit. Care Clin.* 19 (2003) 459–472.
- [2] R.H. Notter, in: C. Lenfant (Ed.), *Lung Surfactants: Basic Science and Clinical Applications*, Marcel Dekker, Inc., New York, 2000, pp. 233–248.
- [3] R.H. Notter, in: C. Lenfant (Ed.), *Lung Surfactants: Basic Science and Clinical Applications*, Marcel Dekker, Inc., New York, 2000, pp. 281–298.
- [4] R.H. Notter, in: C. Lenfant (Ed.), *Lung Surfactants: Basic Science and Clinical Applications*, Marcel Dekker, Inc., New York, 2000, pp. 171–206.
- [5] R. Veldhuizen, K. Nag, S. Orgeig, F. Possmayer, *Biochim. Biophys. Acta* 1408 (1998) 90–108.
- [6] J. Johansson, T. Curstedt, H. Jornvall, *Biochemistry* 30 (1991) 6917–6921.
- [7] J.C. Clark, S.E. Wert, C.J. Bachurski, M.T. Stahlman, B.R. Stripp, T.E. Weaver, J.A. Whitsett, *Proc. Natl. Acad. Sci. U.S.A.* 92 (1995) 7794–7798.
- [8] D.K. Vorbroker, S.A. Proffitt, L.M. Noguee, J.A. Whitsett, *Am. J. Physiol.: Lung Cell. Mol. Physiol.* 12 (1995) L647–L656.
- [9] M.M. Lipp, K.Y.C. Lee, J.A. Zasadzinski, A.J. Waring, *Rev. Sci. Instrum.* 68 (1997) 2574–2582.
- [10] M.L. Longo, A.M. Bisagno, J.A.N. Zasadzinski, R. Bruni, A.J. Waring, *Science* 261 (1993) 453–456.
- [11] L.A.J.M. Creuwels, E.H. Boer, R.A. Demel, L.M.G.V. Golde, H.P. Haagsman, *J. Biol. Chem.* 270 (1995) 16225–16229.
- [12] X.H. Bi, C.R. Flach, J. Perez-Gil, I. Plasencia, D. Andreu, E. Oliveira, R. Mendelsohn, *Biochemistry* 41 (2002) 8385–8395.
- [13] C.R. Flach, A. Gericke, K.M.W. Keough, R. Mendelsohn, *Biochim. Biophys. Acta: Biomembr.* 1416 (1999) 11–20.
- [14] M. Gustafsson, M. Palmblad, T. Curstedt, J. Johansson, S. Schürch, *Biochim. Biophys. Acta: Biomembr.* 1466 (2000) 169–178.
- [15] R. Qanbar, S. Cheng, F. Possmayer, S. Schurch, *Am. J. Physiol.: Lung Cell. Mol. Physiol.* 15 (1996) L572–L580.

- [16] Z. Wang, S.B. Hall, R.H. Notter, J. Lipid Res. 37 (1996) 790–798.
- [17] J. Johansson, T. Szyperski, T. Curstedt, K. Wuthrich, Biochemistry 33 (1994) 6015–6023.
- [18] A. Gericke, C.R. Flach, R. Mendelsohn, Biophys. J. 73 (1997) 492–499.
- [19] C.G. Cochrane, S.D. Revak, A. Merritt, G.P. Heldt, M. Hallman, M.D. Cunningham, D. Easa, A. Pramanik, D.K. Edwards, M.S. Alberts, Am. J. Respir. Crit. Care Med. 153 (1996) 404–410.
- [20] J. Johansson, T. Szyperski, K. Wuthrich, FEBS Lett. 362 (1995) 261–265.
- [21] L.R. McLean, J.E. Lewis, K.A. Hagaman, T.J. Owen, E.R. Matthews, J. Pharmacol. Exp. Therap. 266 (1993) 551–556.
- [22] T. Takei, Y. Hashimoto, T. Aiba, K. Sakai, T. Fujiwara, Biol. Pharm. Bull. 19 (1996) 1247–1253.
- [23] T. Takei, Y. Hashimoto, E. Ohtsubo, K. Sakai, H. Ohkawa, Biol. Pharm. Bull. 19 (1996) 1550–1555.
- [24] J. Johansson, Swiss Med. Week. 133 (2003) 275–282.
- [25] G. Nilsson, M. Gustafsson, G. Vandenbussche, E. Veldhuizen, W.J. Griffiths, J. Sjoval, H.P. Haagsman, J.M. Ruyschaert, B. Robertson, T. Curstedt, J. Johansson, Eur. J. Biochem. 255 (1998) 116–124.
- [26] S.L. Seuryncx, J.A. Patch, A.E. Barron, Chem. Biol. 12 (2005) 77–88.
- [27] C.W. Wu, S.L. Seuryncx, K.Y.C. Lee, A.E. Barron, Chem. Biol. 10 (2003) 1057–1063.
- [28] R.J. Simon, R.S. Kania, R.N. Zuckermann, V.D. Huebner, D.A. Jewell, S. Banville, S. Ng, L. Wang, S. Rosenberg, et al., Proc. Natl. Acad. Sci. U.S.A. 89 (1992) 9367–9371.
- [29] R.N. Zuckermann, J.M. Kerr, S.B.H. Kent, W.H. Moos, J. Am. Chem. Soc. 114 (1992) 10646–10647.
- [30] S. Borman, Chem. Eng. News 76 (1998) 56–57.
- [31] S.M. Miller, R.J. Simon, S. Ng, R.N. Zuckermann, J.M. Kerr, W.H. Moos, Drug Dev. Res. 35 (1995) 20–32.
- [32] P. Armand, K. Kirshenbaum, R.A. Goldsmith, S. Farr-Jones, A.E. Barron, K.T.V. Truong, K.A. Dill, D.F. Mierke, F.E. Cohen, R.N. Zuckermann, E.K. Bradley, Proc. Natl. Acad. Sci. 95 (1998) 4309–4314.
- [33] K. Kirshenbaum, A.E. Barron, R.A. Goldsmith, P. Armand, E.K. Bradley, K.T.V. Truong, K.A. Dill, F.E. Cohen, Proc. Natl. Acad. Sci. 95 (1998) 4303–4308.
- [34] F.J. Walther, J.M. Hernandez-Juviel, L.M. Gordon, A.J. Waring, P. Stenger, J.A. Zasadzinski, Exp. Lung Res. 31 (2005) 563–579.
- [35] A.J. Davis, A.H. Jobe, D. Hafner, M. Ikegami, Am. J. Respir. Crit. Care Med. 157 (1998) 553–559.
- [36] P. Kruger, J.E. Baatz, R.A. Dluhy, M. Losche, Biophys. Chem. 99 (2002) 209–228.
- [37] F. Bringezu, J. Ding, G. Berezinski, J.A. Zasadzinski, Langmuir 17 (2001) 4641–4648.
- [38] S.L. Seuryncx, N.J. Brown, C.W. Wu, K.W. Germino, E.K. Kohlmeier, E.P. Ingenito, M.R. Glucksberg, A.E. Barron, M. Johnson, J. Appl. Physiol. 99 (2005) 624–633.
- [39] G. Putz, J. Goerke, H.W. Tausch, J.A. Clements, J. Appl. Physiol. 76 (1994) 1425–1431.
- [40] A. Cruz, C. Casals, K.M.W. Keough, J. Perez-Gil, Biochem. J. 327 (1997) 133–138.
- [41] M.M. Lipp, K.Y.C. Lee, J.A. Zasadzinski, A.J. Waring, Science 273 (1996) 1196–1199.
- [42] J.E. Baatz, B. Elledge, J.A. Whitsett, Biochemistry 29 (1990) 6714–6720.
- [43] M.A. Oosterlakendijksterhuis, H.P. Haagsman, L.M.G. Vangolde, R.A. Demel, Biochemistry 30 (1991) 8276–8281.
- [44] M.A. Oosterlakendijksterhuis, M. Vaneijk, L.M.G. Vangolde, H.P. Haagsman, Biochim. Biophys. Acta 1110 (1992) 45–50.
- [45] S. Taneva, K. Keough, Biophys. J. 66 (1994) 1157–1158.
- [46] G. Vandenbussche, A. Clercx, M. Clercx, T. Cirstedt, J. Johansson, H. Jornvall, J.-M. Ruyschaert, Biochemistry 31 (1992) 9169–9176.
- [47] A. Cruz, L. Vazquez, M. Velez, J. Perez-Gil, Biophys. J. 86 (2004) 308–320.
- [48] A.S. Dico, J. Hancock, M.R. Morrow, J. Stewart, S. Harris, K.M.W. Keough, Biochemistry 36 (1997) 4172–4177.
- [49] K. Nag, J. Perez-Gil, A. Cruz, K.M.W. Keough, Biophys. J. 71 (1996) 246–256.
- [50] M.A. Oosterlakendijksterhuis, H.P. Haagsman, L.M.G. Vangolde, R.A. Demel, Biochemistry 30 (1991) 10965–10971.
- [51] S.H. Yu, F. Possmayer, Biochim. Biophys. Acta 1046 (1990) 233–241.
- [52] S.-H. Yu, F. Possmayer, Biochim. Biophys. 1167 (1993) 264–271.
- [53] Y. Tanaka, T. Takei, T. Aiba, K. Masuda, A. Kiuchi, T. Fujiwara, J. Lipid Res. 27 (1986) 475–485.
- [54] J.D. Amirkhanian, R. Bruni, A.J. Waring, C. Navar, H.W. Tausch, Biochim. Biophys. Acta 1168 (1993) 315–320.
- [55] J.D. Amirkhanian, R. Bruni, A.J. Waring, H.W. Tausch, Biochim. Biophys. Acta 1096 (1991) 355–360.
- [56] F. Bringezu, J.Q. Ding, G. Berezinski, A.J. Waring, J.A. Zasadzinski, Langmuir 18 (2002) 2319–2325.
- [57] J. Ding, D.Y. Takamoto, A.V. Nahmen, M.M. Lipp, K.Y.C. Lee, A.J. Waring, J.A. Zasadzinski, Biophys. J. 80 (2001) 2262–2272.
- [58] M. Gupta, J.M. Hernandez-Juviel, A.J. Waring, F.J. Walther, Thorax 56 (2001) 871–876.
- [59] M. Gustafsson, G. Vandenbussche, T. Curstedt, J.M. Ruyschaert, J. Johansson, FEBS Lett. 384 (1996) 185–188.
- [60] M. Palmblad, J. Johansson, B. Robertson, T. Curstedt, Biochem. J. 339 (1999) 381–386.
- [61] F.J. Walther, J.M. Hernandez-Juviel, P.E. Mercado, L.M. Gordon, A.J. Waring, Biol. Neonate 82 (2002) 181–187.
- [62] R.V. Diemel, M.M.E. Snel, L.M.G. van Golde, G. Putz, H.P. Haagsman, J.P. Batenburg, Biochemistry 41 (2002) 15007–15016.
- [63] B.M. Discher, K.M. Maloney, D.W. Grainger, S.B. Hall, Biophys. Chem. 101 (2002) 333–345.
- [64] B.D. Fleming, K.M.W. Keough, Chem. Phys. Lipids 49 (1988) 81–86.
- [65] M. Larsson, K. Larsson, T. Nylander, P. Wollmer, Eur. Biophys. J. Biophys. Lett. 31 (2003) 633–636.
- [66] S. Malcharek, A. Hinz, L. Hilterhaus, H.J. Galla, Biophys. J. 88 (2005) 2638–2649.
- [67] R.H. Notter, S. Holcomb, R.D. Mavis, Chem. Phys. Lipids 27 (1980) 305–319.
- [68] S. Ogrieg, C.B. Daniels, Comp. Biochem. Physiol. A 129 (2001) 75–89.
- [69] S. Taneva, K.M.W. Keough, Biochemistry 36 (1997) 912–922.
- [70] A. Tolle, W. Meier, M. Rudiger, K.P. Hofmann, B. Rustow, Chem. Phys. Lipids 114 (2002) 159–168.
- [71] C. Alonso, T. Alig, J. Yoon, F. Bringezu, H. Warriner, J.A. Zasadzinski, Biophys. J. 87 (2004) 4188–4202.
- [72] R.H. Notter, in: C. Lenfant (Ed.), Lung Surfactants: Basic Science and Clinical Applications, vol. 149, Marcel Dekker, New York, 2000, pp. 45–72.
- [73] K.Y.C. Lee, A. Gopal, A. von Nahmen, J.A. Zasadzinski, J. Majewski, G.S. Smith, P.B. Howes, K. Kjaer, J. Chem. Phys. 116 (2002) 774–783.
- [74] C. Ege, M.K. Ratajczak, J. Majewski, K. Kjaer, K.Y.C. Lee, Biophys. J. 91 (2006) L01–L03.
- [75] A. Gopal, K.Y.C. Lee, J. Phys. Chem. B 105 (2001) 10348–10354.
- [76] S. Krol, A. Janshoff, M. Ross, H.-J. Galla, Phys. Chem. Chem. Phys. 2 (2000) 4586–4593.
- [77] D.Y. Takamoto, M.M. Lipp, A.V. Nahmen, K.Y.C. Lee, A.J. Waring, J.A. Zasadzinski, Biophys. J. 81 (2001) 153–169.
- [78] E.J.A. Veldhuizen, J.J. Batenburg, L.M.G.V. Golde, H.P. Haagsman, Biophys. J. 79 (2000) 3164–3171.
- [79] E.M. Scarpelli, E. David, M. Cordova, A.J. Mautone, Am. J. Perinatol. 9 (1992) 414–419.
- [80] C. Ege, M.K. Ratajczak, J. Majewski, K. Kjaer, K.Y.C. Lee, Biophys. J. 91 (2006) L01.
- [81] R.H. Notter, Lung Surfactants: Basic Science and Clinical Applications, vol. 149, Marcel Dekker, New York, 2000.
- [82] E.P. Ingenito, L.M.J. Morris, F.F. Espinosa, R.D. Kamm, M. Johnson, J. Appl. Physiol. 86 (1999) 1702–1714.
- [83] C.W. Wu, Department of Chemical Engineering, Northwestern University, Evanston, IL, 2002.
- [84] A. Gopal, K.Y.C. Lee, J. Phys. Chem. B (2006) (web-released).
- [85] O. Albrecht, H. Gruler, E. Sackmann, J. Colloid Interf. Sci. 79 (1981) 319–338.